Iranian Journal of Numerical Analysis and Optimization
Vol. 16, No. 2, 2026, pp 385–446
https://doi.org/10.22067/ijnao.2025.95479.1732
https://ijnao.um.ac.ir/

CC BY NC

Research Article

Fractal-fractional dynamics of HIV/AIDS: Unveiling the synergistic impact of condoms, prophylaxis, and antiretroviral interventions for epidemic control

G.O. Acheneje[1], J. Amos[1], E. Abah[1], W. Atokolo[1], B.C. Agbata[2], Shyamsunder*[3], A.K. Awasthi[4] and B. Bolaji[1]

Abstract

*Corresponding author

Received 17 September 2025; revised 6 November 2025; accepted 19 November 2025

Godwin Onuche Acheneje, (achenejegodwin@gmail.com)
Jeremiah Amos, (amosjeremiah1997@gmail.com)
Emmanuel Abah, (abahemmanuel1995@gmail.com)
William Atokolo, (williamsatokolo@gmail.com)
Benedict Celestine Agbata, (agbatacelestine92@gmail.com)
Shyamsunder, (skumawatmath@gmail.com)
A.K. Awasthi, (dramitawasthi@gmail.com)
Bolarinwa Bolaji, (bolarinwa.s.bolaji@gmail.com)

[1]Department of Mathematical Sciences, Prince Abubakar Audu University, Anyigba, Nigeria, Laboratory of Mathematical Epidemiology, Prince Abubakar Audu University, Anyigba, Nigeria.
[2]Department of Mathematics and Statistics, Confluence University of Science and Technology, Osara, Kogi State, Nigeria.
[3]Department of Mathematics, SRM University Delhi-NCR, Sonepat-131029, Haryana, India.
[4]Department of Mathematics, School of Chemical Engineering and Physical Sciences, Lovely Professional University, Phagwara, Punjab, India.

How to cite this article
Acheneje, G.O., Amos, J., Abah, E., Atokolo, W., Agbata, B.C., Shyamsunder, Awasthi, A.K. and Bolaji, B. , Fractal-fractional dynamics of HIV/AIDS: Unveiling the synergistic impact of condoms, prophylaxis, and antiretroviral interventions for epidemic control. *Iran. J. Numer. Anal. Optim.*, 2026; 16(2): 385-446. https://doi.org/10.22067/ijnao.2025.95479.1732

HIV/AIDS remains a global health crisis, with over 39 million people living with HIV in 2023, mainly in sub-Saharan Africa. This study presents a novel **fractal-fractional order model** to capture memory effects and heterogeneous transmission patterns in HIV dynamics. Unlike classical integer-order models, it integrates fractional derivatives (for long-term dependencies) and fractal dimensions (for self-similar contact networks). We prove solution positivity, boundedness, and compute the basic reproduction number R_{0H}, with global asymptotic stability at the endemic equilibrium when $R_{0H} > 1$. Sensitivity analysis identifies mortality, AIDS progression, contact rate, and treatment uptake as key R_{0H} drivers. Fitted to South African data (2010–2023), the model estimates $R_{0H} \approx 0.95$ and projects a 28% decline in new infections by 2033 under current trends. Numerical simulations using a second-order Adams–Bashforth scheme show lower fractional orders induce realistic oscillations, outperforming integer-order models in data fit and forecasting. Results underscore that **synergistic scale-up of condoms, PrEP, and ART** is critical to achieving HIV elimination.

AMS subject classifications (2020): 92D30, 34A08, 26A33, 35R11, 37N25, 92C60, 65L05, 35B35

Keywords: Fractal-fractional model; HIV/AIDS transmission dynamics; Basic reproduction number; Sensitivity analysis; Adams–Bashforth scheme.

1 Introduction

Human immunodeficiency virus (HIV) and acquired immunodeficiency syndrome (AIDS) remain among the most significant global public health challenges of the modern era. HIV is a lentivirus that attacks the human immune system, specifically targeting CD4+ T helper cells, which are crucial components of the adaptive immune response [43]. When left untreated, HIV progressively weakens the immune system, leading to AIDS, a condition characterized by opportunistic infections and malignancies that ultimately prove fatal [23]. According to recent epidemiological data, approximately 38 million people worldwide are living with HIV, with sub-Saharan Africa bearing the heaviest burden of the epidemic [45]. The transmission of HIV occurs primarily through unprotected sexual contact, sharing of contaminated needles, mother-to-child transmission during pregnancy, childbirth, or breastfeeding, and transfusion of infected blood products [20]. Understanding these transmission pathways has been fundamental in developing comprehensive prevention strategies that form the cornerstone of global HIV control efforts. Implementing evidence-based prevention interventions has demonstrated remarkable success in reducing HIV incidence rates in various populations and geographical regions [14]. Condom use represents one of the most effective and widely accessible prevention methods for reducing sexual transmission of HIV. When used consistently and correctly, male latex condoms provide

approximately 80–95% protection against HIV transmission during heterosexual intercourse [48]. Female condoms have similarly demonstrated high efficacy rates, offering an additional option for individuals seeking barrier protection methods [25]. The promotion of condom use through comprehensive sexual education programs and widespread distribution campaigns has been associated with significant reductions in HIV incidence across diverse populations [39].

Pre-exposure prophylaxis (PrEP) has emerged as a revolutionary biomedical intervention for HIV prevention among high-risk populations. PrEP involves the daily administration of antiretroviral medications, typically a combination of tenofovir disoproxil fumarate and emtricitabine, to HIV-negative individuals who are at substantial risk of infection [27]. Clinical trials have demonstrated that consistent PrEP use can reduce HIV acquisition risk by up to 99% in sexually active adults [5]. The World Health Organization now recommends PrEP as part of comprehensive HIV prevention programs for individuals at high risk of HIV infection [49]. Post-exposure prophylaxis (PEP) serves as a critical emergency intervention following potential HIV exposure incidents. PEP involves the administration of a 28-day course of antiretroviral therapy (ART) initiated within 72 hours of exposure, with optimal effectiveness achieved when treatment begins within 2 hours [19]. Studies have shown that timely PEP administration can reduce HIV transmission risk by approximately 80%, making it an essential component of comprehensive HIV prevention strategies [18]. PEP protocols are particularly important for healthcare workers experiencing occupational exposures, individuals reporting sexual assault, and those experiencing high-risk sexual or injection drug use exposures [30]. ART has transformed HIV from a uniformly fatal diagnosis to a manageable chronic condition. Modern ART regimens effectively suppress viral replication, restore immune function, and dramatically improve quality of life and survival outcomes for people living with HIV [37]. Furthermore, the concept of treatment as prevention has gained significant recognition, with studies demonstrating that individuals achieving undetectable viral loads through consistent ART adherence cannot transmit HIV sexually, a principle known as "Undetectable = Untransmittable" (U=U) [40]. This breakthrough understanding has profound implications for individual health outcomes and population-level HIV prevention strategies [21].

Mathematical modeling has become increasingly important in understanding infectious disease dynamics and evaluating intervention strategies [12, 34, 33, 17, 1]. Multigroup formulations with stability analysis and optimal control have recently proven effective for regional COVID-19 management [22], motivating our fractal-fractional extension to capture memory-driven HIV persistence in sub-Saharan Africa. Traditional integer-order differential equation models have provided valuable insights into disease transmission patterns and control measures [6]. However, these conventional approaches often fail to capture the complex memory effects and hereditary properties inherent in biological systems, particularly in the context of chronic infections

like HIV [6]. The human immune system exhibits nonlocal temporal correlations and memory-dependent responses that are more accurately described by fractional calculus formulations [38]. Fractional-order differential equations incorporate noninteger derivatives that provide more flexible and realistic representations of biological phenomena characterized by memory and hereditary effects [29]. In HIV dynamics, fractional-order models can better capture the gradual immune system deterioration, the long-term effects of viral persistence, and the complex pharmacokinetic properties of antiretroviral medications [7]. These models have demonstrated superior fitting capabilities compared to classical integer-order models when applied to real-world HIV progression data [24]. Recent advances in fractional calculus have led to the development of fractal-fractional operators, which combine the benefits of fractal geometry and fractional calculus to model complex systems with both memory effects and fractal properties [9]. The fractal-fractional approach is particularly well-suited for modeling biological systems that exhibit self-similar patterns across multiple scales, such as the hierarchical structure of immune system responses and viral population dynamics [10]. These operators provide enhanced flexibility in capturing the intricate dynamics of host-pathogen interactions while maintaining mathematical rigor and computational feasibility [11].

The application of fractal-fractional methods to infectious disease modeling has gained considerable attention in recent literature. Studies have successfully employed these techniques to model various infectious diseases, including tuberculosis, malaria, and COVID-19, demonstrating improved accuracy in predicting disease trajectories and evaluating control strategies [41, 28, 4]. The fractal-fractional framework allows researchers to simultaneously incorporate multiple scales of biological organization, from molecular-level viral dynamics to population-level transmission patterns, providing a more comprehensive understanding of disease progression and intervention effectiveness [31].

In the specific context of HIV/AIDS modeling, integrating fractal-fractional operators offers unique advantages for capturing the multi-scale nature of infection dynamics. The fractal component can account for the spatial heterogeneity in viral distribution within tissues and the scale-invariant properties of immune cell networks, while the fractional component addresses the memory effects associated with immune system priming and antiretroviral drug accumulation [13]. This dual approach enables a more accurate representation of the complex feedback mechanisms governing HIV pathogenesis and treatment responses [35]. Developing robust numerical methods for solving fractal-fractional differential equations has facilitated their practical application in epidemiological modeling. Advanced computational techniques, including spectral methods, finite difference schemes, and machine learning-enhanced algorithms, have been developed to handle the increased mathematical complexity while maintaining computational efficiency [44]. These methodological advances have made fractal-fractional modeling accessible

to researchers investigating complex biological systems, opening new avenues for understanding disease dynamics and optimizing intervention strategies.

Based on the reviewed literature, there exists a significant gap in the mathematical modeling of HIV/AIDS transmission dynamics, particularly in exploring the combined impact of prophylaxis and antiretroviral therapy on reducing disease burden in human populations. This research addresses this gap by employing a novel fractal-fractional order modeling approach, offering a more nuanced analysis of the transmission dynamics compared to traditional integer-order methods.

The remaining part of this manuscript is outlined as follows: In Section 2, the HIV/AIDS integer-order model is presented; Section 3 presents the HIV/AIDS model in fractal-fractional order form. The major analysis of the model is carried out in Section 3. In Section 4,qualitative analysis of the fractal-fractional HIV/AIDS model are presented, and Section 5 contains the concluding remarks of the work.

2 Model formulation

2.1 Key assumptions in model formulation

1. The model presumes a uniformly mixed population where each individual has an equal likelihood of encountering an infected person, as described by the force of infection term λ_H [15].

2. It is assumed that PrEP, PEP, and ART exhibit partial effectiveness, quantified by the efficacy parameters ε_1, ε_2, and η, respectively [26].

3. The model posits that ART lowers the viral load, potentially allowing individuals to revert to a less infectious state (governed by parameter χ), while also reducing the likelihood of transmission (modified by parameter η) [20].

2.2 Model description

The human population (N) is divided into seven mutually exclusive groups (see Figure 1 for a visual overview and Table 1 for parameter definitions): Susceptible individuals (S_H), susceptible

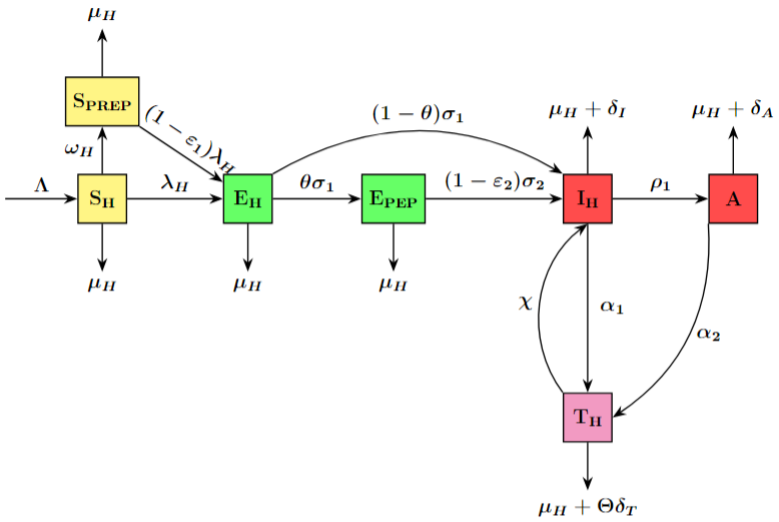

Figure 1: A diagram outlining the epidemiological compartments for HIV/AIDS transmission, depicting groups including susceptible individuals, those on PrEP, exposed individuals, those on PEP, people infected with HIV, those with HIV/AIDS, and various treatment stages [2]

.

individuals on PrEP (S_{PrEP}), exposed individuals (E_H), exposed individuals on PEP (E_{PEP}), individuals infected with HIV only (I_H), individuals with HIV/AIDS (A), and individuals with HIV/AIDS on ART (T_H).

As illustrated in the top-left of Figure 1, new individuals enter the susceptible population at a rate Λ. From S_H, individuals may transition to S_{PrEP} at rate ω_H (top branch) or become exposed (E_H) via the force of infection λ_H (central infection arrow). The force of infection depends on the transmission probability per contact with infectious individuals (I_H, A, or T_H), modulated by contact rate γ_H, condom adherence ς and efficacy Ψ, and number of sexual partners $\gamma > 1$. A natural mortality rate θ_H applies to all compartments (shown as downward arrows in Figure 1).

The parameter η $(0 < \eta < 1)$ reduces transmission from the treated group (T_H) compared to I_H or A (indicated by a lighter infection arrow from T_H in Figure 1). The middle section of Figure 1 shows exposed individuals (E_H) progressing at rate σ_1 either to PEP (E_{PEP}, proportion θ) or directly to I_H (proportion $1-\theta$). PrEP reduces infection risk by factor ε_1, with failure leading to exposure at $(1-\varepsilon_1)\lambda_H$. Similarly, PEP has efficacy ε_2, with failure transitioning individuals to I_H at rate σ_2.

The lower part of Figure 1 depicts disease progression and treatment pathways: HIV-infected individuals (I_H) either initiate ART at rate θ_1 or progress to AIDS (A) at rate ρ_1. Individuals in A enter treatment at rate θ_2. Treated individuals (T_H) experience reduced disease-induced

mortality ($\Theta\delta_T$) and may revert to I_H at rate χ due to treatment interruption or virological failure. Disease-induced mortality rates are δ_I for I_H, δ_A for A, and δ_T for T_H.

A key feature of the model is the reversible treatment pathway: Individuals in the ART group (T_H) transition back to the untreated HIV-infected group (I_H) at rate $\chi > 0$, representing treatment dropout, poor adherence, or virological rebound (see reversible arrow between I_H and T_H in Figure 1). This mechanism ensures the model reflects real-world challenges in sustaining viral suppression and prevents unrealistic assumptions of permanent treatment efficacy.

Table 1: Table of variables and parameters for the HIV/AIDS transmission model.

Variable (Parameter)	**Description**
S_H	Susceptible individuals
S_{PrEP}	Susceptible individuals on PrEP
E_H	Exposed individuals
E_{PEP}	Exposed individuals on PEP
I_H	Individuals infected with HIV only
A	Individuals with HIV/AIDS
T_H	Individuals with HIV/AIDS on ART
Λ	Rate of entry into the susceptible population
λ_H	Force of infection for HIV/AIDS
γ_H	Contact rate between susceptible and infectious individuals
ς	Condom use adherence rate ($0 < \varsigma < 1$)
Ψ	Condom efficacy ($0 < \Psi < 1$)
γ	Number of sexual partners per individual ($\gamma > 1$)
θ_H	Natural mortality rate across all groups
η	Parameter for reduced transmission in the treatment group ($0 < \eta < 1$)
ω_H	Rate of transition to the PrEP group
ε_1	Effectiveness of PrEP ($0 < \varepsilon_1 < 1$)
$(1-\varepsilon_1)\lambda_H$	Failure rate of PrEP leading to exposure
σ_1	Progression rate of exposed individuals
θ	Proportion of exposed individuals using PEP
σ_2	Failure rate of PEP leading to infection
ε_2	Effectiveness of PEP ($0 < \varepsilon_2 < 1$)
θ_1	Rate of transition of HIV-infected individuals to ART
ρ_1	Rate of progression of HIV-infected individuals to the HIV/AIDS group
θ_2	Rate of transition of HIV/AIDS individuals to ART
δ_I	Disease-induced mortality rate for HIV-infected individuals
δ_A	Disease-induced mortality rate for HIV/AIDS individuals
δ_T	Disease-induced mortality rate for individuals in the treatment group
χ	Rate of reversion to the HIV-only group due to reduced viral load
Θ	Parameter for reduced disease-induced mortality in the treatment group

2.3 Model equations

Based on the model description, the system of differential equations governing the HIV/AIDS transmission dynamics in the human population is expressed as

$$\begin{aligned}
\frac{dS_H}{dt} &= \Lambda - (\lambda_H + \omega_H + \theta_H)\, S_H, \\
\frac{dS_{PrEP}}{dt} &= \omega_H S_H - ((1-\varepsilon_1)\lambda_H + \theta_H)\, S_{PrEP}, \\
\frac{dE_H}{dt} &= \lambda_H S_H + (1-\varepsilon_1)\lambda_H S_{PrEP} - (\sigma_1 + \theta_H)\, E_H, \\
\frac{dE_{PEP}}{dt} &= \theta\sigma_1 E_H - ((1-\varepsilon_2)\sigma_2 + \theta_H)\, E_{PEP}, \\
\frac{dI_H}{dt} &= (1-\theta)\sigma_1 E_H + (1-\varepsilon_2)\sigma_2 E_{PEP} - (\theta_1 + \rho_1 + \delta_I + \theta_H)\, I_H + \chi T_H, \\
\frac{dA}{dt} &= \rho_1 I_H - (\theta_2 + \delta_A + \theta_H)\, A, \\
\frac{dT_H}{dt} &= \theta_1 I_H + \theta_2 A - (\chi + \Theta\delta_T + \theta_H)\, T_H,
\end{aligned} \tag{1}$$

where the total population is $N(t) = S_H + S_{PrEP} + E_H + E_{PEP} + I_H + A + T_H$, and the force of infection is defined as $\lambda_H = \frac{(1-\varsigma\Psi)\gamma\gamma_H(I_H + A + \eta T_H)}{N}$ for the HIV/AIDS model in (1).

2.4 Background materials

The manuscript relies on fractal-fractional operator definitions, which we outline first. Let τ represents the fractional order, and let ψ denotes the fractal dimension. One assumes a function $y(t)$ is continuous and possesses fractal differentiability on the interval (a, b) with respect to ψ. These definitions are detailed in references [8, 36].

Definition 1. [8] The Caputo fractional differential operator employs the Mittag-Leffler kernel to define the fractal-fractional derivative of a function $y(t)$ at order τ and fractal dimension ψ as follows:

$$FFH_{0,t}^{\tau,\psi} y(t) = \frac{AB(\tau)}{1-\tau} \int_a^t E_\tau \left[\frac{-\tau}{1-\tau}(t-s)^\tau \right] \frac{dy(s)}{ds^\psi}\, ds, \quad t \geq a \geq 0, \tag{2}$$

where $\tau, \psi \in (0,1]$, and $AB(\tau) = 1 - \tau + \frac{\tau}{\Gamma(\tau)}$ is the normalization function satisfying $AB(0) = AB(1) = 1$. The fractal derivative is defined as

$$\frac{dx(t)}{dt^{\psi}} = \lim_{s \to t} \frac{x(s) - x(t)}{s^{\psi} - t^{\psi}}.$$

The Mittag-Leffler function is given by

$$E_{\tau}(z) = \sum_{k=0}^{\infty} \frac{z^k}{\Gamma(\tau k + 1)}, \quad z, \tau \in \mathbb{C}, \quad \tau > 0,$$

where $\mathbb{C}$ is the set of complex numbers.

Definition 2. [8, 36] The fractal-fractional integral with the Mittag-Leffler kernel in the Caputo sense, of order τ and dimension ψ, is defined as

$$\begin{aligned} FFH_{0,t}^{\tau,\psi} y(t) =& \frac{\psi(1-\tau) t^{\psi-1} y(t)}{AB(\tau)} \\ &+ \frac{\tau\psi}{AB(\tau)\,\Gamma(\tau)} \int_a^t (t-s)^{\tau-1} s^{\psi-1} y(s)\, ds, \quad t \geq a \geq 0. \end{aligned} \tag{3}$$

Definition 3. [8] For $x \in C((a,b), \mathbb{R})$, the fractal Laplace transform of order ψ is given by

$${}^{F}L_p^{\psi} x(t) = \int_0^{\infty} x(t) \exp(-pt) t^{\psi-1}\, dt. \tag{4}$$

Lemma 1. [36] Consider the fractal-fractional initial value problem:

$$FFH_{0,t}^{\tau,\psi} x(t) = G(t, x(t)), \quad t \in [0,T], \quad \tau, \psi \in (0,1], \quad x(0) = x_0. \tag{5}$$

This can be equivalently expressed as

$$FFH_{0,t}^{\tau,\psi} x(t) = \psi t^{\psi-1} G(t, x(t)), \quad t \in [0,T], \quad \tau, \psi \in (0,1], \quad x(0) = x_0. \tag{6}$$

The corresponding integral equation for the solution is

$$\begin{aligned} x(t) =& x(0) + \frac{\psi t^{\tau-1}(1-\tau) G(t, x(t))}{AB(\tau)} \\ &+ \frac{\psi\tau}{AB(\tau)\Gamma(\tau)} \int_0^t s^{\psi-1} (t-s)^{\tau-1} G(s, x(s))\, ds. \end{aligned} \tag{7}$$

Lemma 2 (Banach fixed point theorem [3])**.** In a Banach space X, let $D \subset X, D \neq \emptyset$ be a closed subset. An operator $P : D \to D$ has a unique fixed point in D if it satisfies the contraction condition.

Lemma 3 (Krasnoselskii's fixed point theorem)**.** [42] Let $D \subset Y$ be a nonempty, closed, and convex subset of a Banach space Y. For operators P and Q such that

1. $Pu + Qv \in D$ whenever $u, v \in D$,
2. Q is compact and continuous,
3. P is a contraction mapping,

there exists $k \in D$ such that $k = Pk + Qk$.

3 Analysis of HIV/AIDS model

The fractal-fractional derivative operator is applied to advance the HIV/AIDS model within the Mittag-Leffler kernel framework, with $\tau \in (0, 1]$ and $\psi \in [0, 1]$, as follows:

$$\begin{aligned}
FFH^{\tau,\psi}_{0,t} S_H(t) &= G_1\left(t, S_H(t), S_{PREP}(t), E_H(t), E_{PEP}(t), I_H(t), A(t), T_H(t)\right),\\
FFH^{\tau,\psi}_{0,t} S_{PREP}(t) &= G_2\left(t, S_H(t), S_{PREP}(t), E_H(t), E_{PEP}(t), I_H(t), A(t), T_H(t)\right),\\
FFH^{\tau,\psi}_{0,t} E_H(t) &= G_3\left(t, S_H(t), S_{PREP}(t), E_H(t), E_{PEP}(t), I_H(t), A(t), T_H(t)\right),\\
FFH^{\tau,\psi}_{0,t} E_{PEP}(t) &= G_4\left(t, S_H(t), S_{PREP}(t), E_H(t), E_{PEP}(t), I_H(t), A(t), T_H(t)\right),\\
FFH^{\tau,\psi}_{0,t} I_H(t) &= G_5\left(t, S_H(t), S_{PREP}(t), E_H(t), E_{PEP}(t), I_H(t), A(t), T_H(t)\right),\\
FFH^{\tau,\psi}_{0,t} A(t) &= G_6\left(t, S_H(t), S_{PREP}(t), E_H(t), E_{PEP}(t), I_H(t), A(t), T_H(t)\right),\\
FFH^{\tau,\psi}_{0,t} T_H(t) &= G_7\left(t, S_H(t), S_{PREP}(t), E_H(t), E_{PEP}(t), I_H(t), A(t), T_H(t)\right),
\end{aligned} \tag{8}$$

where

$G_i = G_i\left(t, S_H(t), S_{PREP}(t), E_H(t), E_{PEP}(t), I_H(t), A(t), T_H(t)\right).$

The functions G_i for $i = 1, 2, \ldots, 7$ are defined as follows:

$$\begin{aligned}
G_1 &= \Lambda - \left(\lambda_H + \omega_H + \theta_H\right) S_H,\\
G_2 &= \omega_H S_H - \left((1-\varepsilon_1)\lambda_H + \theta_H\right) S_{PREP},\\
G_3 &= \lambda_H S_H + (1-\varepsilon_1)\lambda_H S_{PREP} - \left(\sigma_1 + \theta_H\right) E_H,\\
G_4 &= \theta\sigma_1 E_H - \left((1-\varepsilon_2)\sigma_2 + \theta_H\right) E_{PEP},\\
G_5 &= (1-\theta)\sigma_1 E_H + (1-\varepsilon_2)\sigma_2 E_{PEP} - \left(\theta_1 + \rho_1 + \delta_I + \theta_H\right) I_H + \chi T_H,\\
G_6 &= \rho_1 I_H - \left(\theta_2 + \delta_A + \theta_H\right) A,\\
G_7 &= \theta_1 I_H + \theta_2 A - \left(\chi + \Theta\delta_T + \theta_H\right) T_H.
\end{aligned} \tag{9}$$

with initial conditions

$$S_{H0} \geq 0, S_{PREP0} \geq 0, E_{H0} \geq 0, E_{PEP0} \geq 0, I_{H0} \geq 0, A_0 \geq 0, T_{H0} \geq 0.$$

The fractal-fractional FF-HIV/AIDS model is labeled as (8). If $\tau = 1$, then the model reduces to an integer-order system as in (1). If $\psi = 1$, then it simplifies to a fractional-order HIV/AIDS model.

3.1 Positivity of the model solution

Define the nonnegative region
$\mathbb{R}_+^7 = \left\{ G \in \mathbb{R}_+^7 : G \geq 0 \text{ and } (S_H, S_{PREP}, E_H, E_{PEP}, I_H, A, T_H)^T \right\}$,
where $(\cdot)^T$ denotes the vector transpose.

Theorem 1. *G satisfies boundedness in $\mathbb{R}_+^7$ in addition to being nonnegative for the solution of the FF-HIV/AIDS model described by (8).*

Proof. For $t \in (0, \infty)$, the existence and uniqueness of the FF-HIV/AIDS model (8) is obtained.

This result follows from the Lipschitz continuity of the right-hand side functions $\mathbf{G}(t, \mathbf{X})$ in the bounded region Ω_H, which ensures that the associated integral operator is a contraction mapping on a suitable Banach space of continuous functions. The Lipschitz condition holds because all transition rates (infection, progression, treatment, mortality) are either linear or bilinear in the state variables and are uniformly bounded due to population saturation and density-dependent transmission. Under these conditions, the Banach fixed point theorem guarantees a unique solution on any finite time interval, which can be extended globally by continuation.

Consequently, The nonnegative region $\mathbb{R}_+^7$ represents a positive invariant region according to the presented content. Our research used the FF-HIV/AIDS model described in (8) as the basis for our analysis:

$$\begin{aligned}
&FFH_{0,t}^{\tau,\psi} S_H(t) = \Lambda \geq 0,\\
&FFH_{0,t}^{\tau,\psi} S_{PREP}(t) = \omega_H S_H \geq 0,\\
&FFH_{0,t}^{\tau,\psi} E_H(t) = \lambda_H S_H + (1-\varepsilon_1)\lambda_H S_{PREP} \geq 0,\\
&FFH_{0,t}^{\tau,\psi} E_{PEP}(t) = \theta\sigma_1 E_H \geq 0,\\
&FFH_{0,t}^{\tau,\psi} I_H(t) = (1-\theta)\sigma_1 E_H + (1-\varepsilon_2)\sigma_2 E_{PEP} + \chi T_H \geq 0,\\
&FFH_{0,t}^{\tau,\psi} A(t) = \rho_1 I_H \geq 0,
\end{aligned}$$

$$FFH_{0,t}^{\tau,\psi}T_H(t) = \theta_1 I_H + \theta_2 A \geq 0. \tag{10}$$

If $(S_H, S_{PREP}, E_H, E_{PEP}, I_H, A, T_H) \in \mathbb{R}_+^7$, then from the time interval from (10) solution G remains prevented from escaping through the hyper planes.

Consequently, $\mathbb{R}_+^7$ is a positively invariant and $N = S_H + S_{PREP} + E_H + E_{PEP} + I_H + A + T_H$.

So from the FF-HIV/AIDS model (8), we obtain

$$\left\{FFH_{0,t}^{\tau,\psi}N\left(t\right)\left(t\right) = \Lambda - \theta_H N - \delta_I I_H - \delta_A A - \Theta\delta_T T_H\right\}. \tag{11}$$

Using the fractal Laplace transform in (3), we conclude that $N(t) \leq \frac{\Lambda}{\theta_H}$ as $t \to \infty$.

So we now have the biological range of values of the FF-HIV/AIDS model (8) as follows:

$$\left\{\begin{array}{l}(S_H, S_{PREP}, E_H, E_{PEP}, I_H, A, T_H) \in R^7 \\ : S_H, S_{PREP}, E_H, E_{PEP}, I_H, A, T_H \geq 0\end{array}\right\}$$

and $N(t) \leq \frac{\Lambda}{\theta_H}$.

This shows that the above model is biologically feasible.

The biological implication of these fractal-fractional theorems is that they ensure the model behaves realistically over time: No population compartment can become negative, and the total population remains bounded by a natural ceiling determined by birth rate (Λ) and natural death rate (θ_H). This reflects real-world demographics where populations grow but are limited by resources and mortality. The positive invariance property means that once individuals enter a disease state (e.g., exposed, infected, or under treatment), the model correctly tracks their progression without artificial loss or gain. Furthermore, the boundedness result implies long-term stability of the population size, which is crucial for sustainable public health planning and intervention forecasting—especially in high-burden regions like sub-Saharan Africa, where uncontrolled population growth in models could lead to misleading predictions of disease spread or intervention impact.

□

3.2 Basic reproduction number of the HIV/AIDS model

The basic reproduction number, R_{0H}, is computed using the next-generation matrix method [47], a standard approach for compartmental epidemic models as developed by Van Den Driessche and Watmough. This method involves separating the population into infected compartments and constructing the Jacobian matrices of new infections ($\mathcal{F}$) and transitions between infected states ($\mathcal{V}$) at the disease-free equilibrium. The spectral radius of the next-generation matrix $\mathcal{F}\mathcal{V}^{-1}$

yields R_{0H}, representing the expected number of secondary HIV infections produced by a single infected individual in a fully susceptible population over their infectious period.

Therefore, $R_{0H} = \rho\left(FV^{-1}\right)$, where F is defined as the matrix of infection and V is defined as the matrix of the transient terms.

$$F = \begin{bmatrix} 0 & 0 & \frac{(1-\varsigma\Psi)\gamma\gamma_H Z_2}{Z_1} & \frac{(1-\varsigma\Psi)\gamma\gamma_H Z_2}{Z_1} & \frac{\eta(1-\varsigma\Psi)\gamma\gamma_H Z_2}{Z_1} \\ 0 & 0 & 0 & 0 & 0 \\ 0 & 0 & 0 & 0 & 0 \\ 0 & 0 & 0 & 0 & 0 \\ 0 & 0 & 0 & 0 & 0 \end{bmatrix},$$

$$V = \begin{bmatrix} P_1 & 0 & 0 & 0 & 0 \\ -v_{21} & P_2 & 0 & 0 & 0 \\ -v_{31} & -v_{32} & P_3 & 0 & -\chi \\ 0 & 0 & -\rho_1 & P_4 & 0 \\ 0 & 0 & -\theta_1 & -\theta_2 & P_5 \end{bmatrix},$$

$$FV^{-1} = \begin{bmatrix} \widehat{F_1} & \widehat{F_2} & \widehat{F_3} & \widehat{F_4} & \widehat{F_5} \\ 0 & 0 & 0 & 0 & 0 \\ 0 & 0 & 0 & 0 & 0 \\ 0 & 0 & 0 & 0 & 0 \\ 0 & 0 & 0 & 0 & 0 \\ 0 & 0 & 0 & 0 & 0 \end{bmatrix},$$

where

$$v_{21} = \theta\sigma_1,\ v_{31} = (1-\theta)\,\sigma_1,\ v_{32} = (1-\varepsilon_2)\,\sigma_2,$$

$$P_1 = (\sigma_1 + \theta_H), P_2 = ((1-\varepsilon_2)\,\sigma_2 + \theta_H), P_3 = (\theta_1 + \rho_1 + \delta_I + \theta_H),$$

$$P_4 = (\theta_2 + \delta_A + \theta_H), P_5 = (\chi + \Theta\delta_T + \theta_H),\ Z_1 = (\omega_H + \theta_H),\ Z_2 = ((1-\varepsilon_1)\,\omega_H + \theta_H).$$

$$\widehat{F_1} = \frac{\gamma_H\ (\psi\,\varsigma - 1)\,(P_2\,v_{31} + v_{21}\,v_{32})\,Z_2\ ((\eta\,\theta_1 + P_5)\,P_4 + \rho_I\ (\eta\,\theta_2 + P_5))\,\gamma}{P_1\ ((-P_3\,P_5 + \chi\,\theta_1)\,P_4 + \chi\,\theta_2\,\rho_I)\,P_2\,Z_1},$$
$$\widehat{F_2} = \frac{\gamma\,\gamma_H\ ((\eta\,\theta_1 + P_5)\,P_4 + \rho_I\ (\eta\,\theta_2 + P_5))\,v_{32}\ (\psi\,\varsigma - 1)\,Z_2}{P_2\ ((-P_3\,P_5 + \chi\,\theta_1)\,P_4 + \chi\,\theta_2\,\rho_I)\,Z_1},$$
$$\widehat{F_3} = \frac{\gamma\ (\psi\,\varsigma - 1)\,((\eta\,\theta_1 + P_5)\,P_4 + \rho_I\ (\eta\,\theta_2 + P_5))\,Z_2\,\gamma_H}{Z_1\ ((-P_3\,P_5 + \chi\,\theta_1)\,P_4 + \chi\,\theta_2\,\rho_I)},$$
$$\widehat{F_4} = -\frac{\gamma\ (\psi\,\varsigma - 1)\,((\theta_1 - \theta_2)\,\chi - P_3\ (\eta\,\theta_2 + P_5))\,Z_2\,\gamma_H}{Z_1\ ((P_4\,\theta_1 + \theta_2\,\rho_I)\,\chi - P_3\,P_4\,P_5)},$$
$$\widehat{F_5} = \frac{((P_3\,\eta + \chi)\,P_4 + \rho_I\,\chi)\,\gamma\ (\psi\,\varsigma - 1)\,Z_2\,\gamma_H}{Z_1\ ((-P_3\,P_5 + \chi\,\theta_1)\,P_4 + \chi\,\theta_2\,\rho_I)}.$$

The dominant eigenvalue of FV^{-1} which is the basic reproduction number of the HIV/AIDS model is given as

$$R_{0H} = \frac{(1 - \varsigma\psi)\,\gamma_H\,\gamma\,((\eta\,\theta_1 + P_5)\,P_4 + \rho_I\ (\eta\,\theta_2 + P_5))\,(P_2\,v_{31} + v_{21}\,v_{32})\,Z_2}{Z_1 P_1\,P_2\ (P_4\,(P_3\,P_5 - \chi\,\theta_1) - \theta_2\,\rho_I\,\chi)}. \tag{12}$$

4 Qualitative analysis of the fractal-fractional HIV/AIDS model

To demonstrate the qualitative results of the HIV/AIDS model (8), we need the specified Banach space. Let $\tau = [0, T]$ represent the time interval of all continuous real-valued functions denoted as $Y = C\left(\tau \times \mathbb{R}^7, \mathbb{R}\right)$ equipped with the norm

$$\begin{aligned}
\|x\| &= \|(S_H, S_{PREP}, E_H, E_{PEP}, I_H, A, T_H)\| \\
&= \|S_H\| + \|S_{PREP}\| + \|E_H\| + \|E_{PEP}\| + \|I_H\| + \|A\| + \|T_H\|, \\
\|S_H\| &= \sup_{t\in\tau} |S_H(t)| = A_{h1}, \\
\|S_{PREP}\| &= \sup_{t\in\tau} |S_{PREP}(t)| = A_{h2}, \\
\|E_H\| &= \sup_{t\in\tau} |E_H(t)| = A_{h3}, \\
\|E_{PEP}\| &= \sup_{t\in\tau} |E_{PEP}(t)| = A_{h4}, \\
\|I_H\| &= \sup_{t\in\tau} |I_H(t)| = A_{h5}, \\
\|A\| &= \sup_{t\in\tau} |A(t)| = A_{h6}, \\
\|T_H\| &= \sup_{t\in\tau} |T_H(t)| = A_{h7}.
\end{aligned} \tag{13}$$

Here $(S_H, S_{PREP}, E_H, E_{PEP}, I_H, A, T_H) \in X$. Let $G \in X$ and $x \in C(\tau, \mathbb{R})$. Then, the HIV/AIDS model (1) can be expressed as

$$\begin{cases} FFH_{0,t}^{\tau,\psi} x(t) = G(t, x(t)), \quad t \in [0, T], \tau, \psi \in (0, 1], \\ x(0) = x_0, \end{cases}$$

where

$$x(t) = \begin{pmatrix} S_H(t) \\ S_{PREP}(t) \\ E_H(t) \\ E_{PEP}(t) \\ I_H(t) \\ A(t) \\ T_H(t) \end{pmatrix}, \quad x(0) = \begin{pmatrix} S_H(0) \\ S_{PREP}(0) \\ E_H(0) \\ E_{PEP}(0) \\ I_H(0) \\ A(0) \\ T_H(0) \end{pmatrix}, \quad G(t, x(t)) = \begin{pmatrix} G_1(t, S_H(t)) \\ G_2(t, S_{PREP}(t)) \\ G_3(t, E_H(t)) \\ G_4(t, E_{PEP}(t)) \\ G_5(t, I_H(t)) \\ G_6(t, A(t)) \\ G_7(t, T_H(t)) \end{pmatrix}. \tag{14}$$

The solution of problem (13) corresponds to this integral equation when G_i, $i = 1, 2, \ldots, 7$, are defined as in (8):

$x(t) = x(0) + \frac{\psi t^{\tau-1}(1-\tau)G(t,x(t))}{AB(\tau)} + \frac{\psi\tau}{AB(\tau)\Gamma(\tau)} \int_0^t s^{\psi-1}(t-s)^{\tau-1} G(s, x(s))\, ds,$

We simplify the calculations by introducing the following symbols in this work:

$$\begin{aligned} G_1(t, S_H(t)) &= G_1\left(t, S_H(t), S_{PREP}(t), E_H(t), E_{PEP}(t), I_H(t), A(t), T_H(t)\right), \\ G_2(t, S_{PREP}(t)) &= G_2\left(t, S_H(t), S_{PREP}(t), E_H(t), E_{PEP}(t), I_H(t), A(t), T_H(t)\right), \\ G_3(t, E_H(t)) &= G_3\left(t, S_H(t), S_{PREP}(t), E_H(t), E_{PEP}(t), I_H(t), A(t), T_H(t)\right), \\ G_4(t, E_{PEP}(t)) &= G_4\left(t, S_H(t), S_{PREP}(t), E_H(t), E_{PEP}(t), I_H(t), A(t), T_H(t)\right), \\ G_5(t, I_H(t)) &= G_5\left(t, S_H(t), S_{PREP}(t), E_H(t), E_{PEP}(t), I_H(t), A(t), T_H(t)\right), \\ G_6(t, A(t)) &= G_6\left(t, S_H(t), S_{PREP}(t), E_H(t), E_{PEP}(t), I_H(t), A(t), T_H(t)\right), \\ G_7(t, T_H(t)) &= G_7\left(t, S_H(t), S_{PREP}(t), E_H(t), E_{PEP}(t), I_H(t), A(t), T_H(t)\right). \end{aligned} \tag{15}$$

The FF-HIV/AIDS model (8) represents the following set of Volterra integral equations according to Lemma 2:

$$\begin{aligned} S_H(t) = S_H(0) &+ \frac{\psi t^{\tau-1}(1-\tau)G_1(t, S_H(t))}{AB(\tau)} \\ &+ \frac{\psi\tau}{AB(\tau)\Gamma(\tau)} \int_0^t s^{\psi-1}(t-s)^{\tau-1} G_1(s, S_H(s))\, ds, \end{aligned}$$

$$
\begin{aligned}
S_{PREP}(t) &= S_{PREP}(0) + \frac{\psi t^{\tau-1}(1-\tau)G_2(t, S_{PREP}(t))}{AB(\tau)} \\
&\quad + \frac{\psi\tau}{AB(\tau)\Gamma(\tau)} \int_0^t s^{\psi-1}(t-s)^{\tau-1} G_2(s, S_{PREP}(s))\, ds, \\
E_H(t) &= E_H(0) + \frac{\psi t^{\tau-1}(1-\tau)G_3(t, E_H(t))}{AB(\tau)} \\
&\quad + \frac{\psi\tau}{AB(\tau)\Gamma(\tau)} \int_0^t s^{\psi-1}(t-s)^{\tau-1} G_3(s, E_H(s))\, ds, \\
E_{PEP}(t) &= E_{PEP}(0) + \frac{\psi t^{\tau-1}(1-\tau)G_4(t, E_{PEP}(t))}{AB(\tau)} \\
&\quad + \frac{\psi\tau}{AB(\tau)\Gamma(\tau)} \int_0^t s^{\psi-1}(t-s)^{\tau-1} G_4(s, E_{PEP}(s))\, ds, \\
I_H(t) &= I_H(0) + \frac{\psi t^{\tau-1}(1-\tau)G_5(t, I_H(t))}{AB(\tau)} \\
&\quad + \frac{\psi\tau}{AB(\tau)\Gamma(\tau)} \int_0^t s^{\psi-1}(t-s)^{\tau-1} G_5(s, I_H(s))\, ds, \\
A(t) &= A(0) + \frac{\psi t^{\tau-1}(1-\tau)G_6(t, A(t))}{AB(\tau)} \\
&\quad + \frac{\psi\tau}{AB(\tau)\Gamma(\tau)} \int_0^t s^{\psi-1}(t-s)^{\tau-1} G_6(s, A(s))\, ds, \\
T_H(t) &= T_H(0) + \frac{\psi t^{\tau-1}(1-\tau)G_7(t, T_H(t))}{AB(\tau)} \\
&\quad + \frac{\psi\tau}{AB(\tau)\Gamma(\tau)} \int_0^t s^{\psi-1}(t-s)^{\tau-1} G_7(s, T_H(s))\, ds.
\end{aligned} \tag{16}
$$

In view of (16), we define an operator,$\iota : X \to X$, where

$$
\begin{aligned}
\iota &= (\iota_1, \iota_2, \iota_3, \iota_4, \iota_5, \iota_6, \iota_7), \\
(\iota_1, S_H)(t) &= S_H(0) + \frac{\psi t^{\tau-1}(1-\tau)G_1(t, S_H(t))}{AB(\tau)} \\
&\quad + \frac{\psi\tau}{AB(\tau)\Gamma(\tau)} \int_0^t s^{\psi-1}(t-s)^{\tau-1} G_1(s, S_H(s))\, ds, \\
(\iota_2, S_{PREP})(t) &= S_{PREP}(0) + \frac{\psi t^{\tau-1}(1-\tau)G_2(t, S_{PREP}(t))}{AB(\tau)} \\
&\quad + \frac{\psi\tau}{AB(\tau)\Gamma(\tau)} \int_0^t s^{\psi-1}(t-s)^{\tau-1} G_2(s, S_{PREP}(s))\, ds, \\
(\iota_3, E_H)(t) &= E_H(0) + \frac{\psi t^{\tau-1}(1-\tau)G_3(t, E_H(t))}{AB(\tau)} \\
&\quad + \frac{\psi\tau}{AB(\tau)\Gamma(\tau)} \int_0^t s^{\psi-1}(t-s)^{\tau-1} G_3(s, E_H(s))\, ds,
\end{aligned}
$$

$$
\begin{aligned}
(\iota_4, E_{PEP})(t) &= E_{PEP}(0) + \frac{\psi t^{\tau-1}(1-\tau)G_4(t, E_{PEP}(t))}{AB(\tau)} \\
&\quad + \frac{\psi\tau}{AB(\tau)\Gamma(\tau)} \int_0^t s^{\psi-1}(t-s)^{\tau-1} G_4(s, E_{PEP}(s))\, ds, \\
(\iota_5, I_H)(t) &= I_H(0) + \frac{\psi t^{\tau-1}(1-\tau)G_5(t, I_H(t))}{AB(\tau)} \\
&\quad + \frac{\psi\tau}{AB(\tau)\Gamma(\tau)} \int_0^t s^{\psi-1}(t-s)^{\tau-1} G_5(s, I_H(s))\, ds, \\
(\iota_6, A)(t) &= A(0) + \frac{\psi t^{\tau-1}(1-\tau)G_6(t, A(t))}{AB(\tau)} \\
&\quad + \frac{\psi\tau}{AB(\tau)\Gamma(\tau)} \int_0^t s^{\psi-1}(t-s)^{\tau-1} G_6(s, A(s))\, ds, \\
(\iota_7, T_H)(t) &= T_H(0) + \frac{\psi t^{\tau-1}(1-\tau)G_7(t, T_H(t))}{AB(\tau)} \\
&\quad + \frac{\psi\tau}{AB(\tau)\Gamma(\tau)} \int_0^t s^{\psi-1}(t-s)^{\tau-1} G_7(s, T_H(s))\, ds. \qquad (17)
\end{aligned}
$$

We transform the examined model into a fixed point problem for fixed point theory investigation: $x = \iota x$. This will apply to create a fixed point theory. Our next section demonstrates the FF-HIV/AIDS model (8) achieves a single solution.

Theorem 2. Let $G \in Y$ satisfy the assumption B_1. There exists a constant $L_{\max} = \max\{L_1, L_2, L_3, L_4, L_5, L_6, L_7\}$, such that

$$
\begin{aligned}
&\Big| G\left(t, S_H(t), S_{PREP}(t), E_H(t), E_{PEP}(t), I_H(t), A(t), T_H(t)\right) \\
&\quad - G\left(t, S_H^*(t), S_{PREP}^*(t), E_H^*(t), E_{PEP}^*(t), I_H^*(t), A^*(t), T_H^*(t)\right) \Big| \\
&\leq L_{\max} \begin{pmatrix} |S_H - S_H^*| + |S_{PREP} - S_{PREP}^*| + |E_H - E_H^*| \\ \quad + |E_{PEP} - E_{PEP}^*| + |I_H - I_H^*| + |A - A^*| + |T_H - T_H^*| \end{pmatrix}.
\end{aligned}
$$

For any
$S_H(t), S_{PREP}(t), E_H(t), E_{PEP}(t), I_H(t), A(t), T_H(t) \in X$ and $t \in \tau$, and
$\left(\psi(1-\tau)T_{\min}^{\tau-1} + \frac{\tau T^{\tau+\psi-1}\Gamma(\psi+1)}{\Gamma(\tau+\psi)}\right)\frac{L_{\max}}{AB(\tau)} < 1$, then the FF-HIV/AIDS model (8) has a unique solution.

Proof. Let D_{Z1} be a bounded, closed, and convex subset defined as
$D_{Z1} = \left\{ \begin{array}{l} (S_H(t), S_{PREP}(t), E_H(t), E_{PEP}(t), I_H(t), A(t), T_H(t)) \in X : \\ \|(S_H, S_{PREP}, E_H, E_{PEP}, I_H, A, T_H)\| \leq Z_1 \end{array} \right\}$, with radius
$\frac{\sigma_{\max} + \left(\psi(1-\tau)T_{\min}^{\psi-1} + \frac{\tau T^{\tau+\psi-1}\Gamma(\psi+1)}{\Gamma(\tau+\psi)}\right)\frac{G_{\max^*}}{AB(\tau)}}{1 - \left(\psi(1-\tau)T_{\min}^{\psi-1} + \frac{\tau T^{\tau+\psi-1}\Gamma(\psi+1)}{\Gamma(\tau+\psi)}\right)\frac{L_{\max^*}}{AB(\tau)}}$, where

$\sigma_{\max} = \max\{S_{H0}(t), S_{PREP0}(t), E_{H0}(t), E_{PEP0}(t), I_{H0}(t), A_0(t), T_{H0}(t)\}$, and let $\sup_{t\in\tau} |G_i(s,0)| = G_i^* < +\infty, \quad i = 1,2,3,4,5,6,7.$

First, we show that $\iota D_{Z1} \subset D_{Z1}$. For any $(S_H(t), S_{PREP}(t), E_H(t), E_{PEP}(t), I_H(t), A(t), T_H(t)) \in D_{Z1},\ t \in \tau$, we obtain

$$\begin{aligned}
|(\iota_1 S_H)(t)| &\le |S_H(0)| + \frac{\psi t^{\tau-1}(1-\tau)}{AB(\tau)} |G_1(t, S_H(t))| \\
&\quad + \frac{\tau\psi}{AB(\tau)\Gamma(\tau)} \int_0^t s^{\psi-1}(t-s)^{\tau-1} |G_1(s, S_H(s))|\, ds \\
&\le |S_H(0)| + \frac{\psi t^{\tau-1}(1-\tau)}{AB(\tau)} [L_1 (|S_H(t)| + |S_{PREP}(t)| + |E_H(t)| \\
&\quad + |E_{PEP}(t)| + |I_H(t)| + |A(t)| + |T_H(t)|) + G_1^*] \qquad (18) \\
&\quad + \frac{\tau\psi}{AB(\tau)\Gamma(\tau)} \int_0^t s^{\psi-1}(t-s)^{\tau-1} [L_1 (|S_H(s)| + |S_{PREP}(s)| \\
&\quad + |E_H(s)| + |E_{PEP}(s)| + |I_H(s)| + |A(s)| + |T_H(s)|) + G_1^*]\, ds \\
&\le S_{H0} + \left(\frac{\psi(1-\tau)T^{\tau-1}}{AB(\tau)} + \frac{\tau T^{\tau+\psi-1}\Gamma(\psi+1)}{AB(\tau)\Gamma(\tau+\psi)} \right) \\
&\quad \times [L_1 (\|S_H\| + \|S_{PREP}\| + \|E_H\| + \|E_{PEP}\| + \|I_H\| + \|A\| \qquad (19) \\
&\quad + \|T_H\|) + G_1^*]\,. \qquad (20)
\end{aligned}$$

Thus, $\|\iota_1 S_H\| \le S_{H0} + \left(\frac{\psi(1-\tau)T_{\min}^{\psi-1}}{AB(\tau)} + \frac{\tau T^{\tau+\psi-1}\Gamma(\psi+1)}{AB(\tau)\Gamma(\tau+\psi)} \right) [L_1 Z_1 + G_1^*]\,.$

Similarly, for $i = 2, 3, \ldots, 7$, we have

$$\begin{aligned}
\|\iota_2 S_{PREP}\| &\le S_{PREP0} + \left(\frac{\psi(1-\tau)T_{\min}^{\psi-1}}{AB(\tau)} + \frac{\tau T^{\tau+\psi-1}\Gamma(\psi+1)}{AB(\tau)\Gamma(\tau+\psi)} \right) [L_2 Z_2 + G_2^*]\,, \\
\|\iota_3 E_H\| &\le E_{H0} + \left(\frac{\psi(1-\tau)T_{\min}^{\psi-1}}{AB(\tau)} + \frac{\tau T^{\tau+\psi-1}\Gamma(\psi+1)}{AB(\tau)\Gamma(\tau+\psi)} \right) [L_3 Z_3 + G_3^*]\,, \\
\|\iota_4 E_{PEP}\| &\le E_{PEP0} + \left(\frac{\psi(1-\tau)T_{\min}^{\psi-1}}{AB(\tau)} + \frac{\tau T^{\tau+\psi-1}\Gamma(\psi+1)}{AB(\tau)\Gamma(\tau+\psi)} \right) [L_4 Z_4 + G_4^*]\,, \\
\|\iota_5 I_H\| &\le I_{H0} + \left(\frac{\psi(1-\tau)T_{\min}^{\psi-1}}{AB(\tau)} + \frac{\tau T^{\tau+\psi-1}\Gamma(\psi+1)}{AB(\tau)\Gamma(\tau+\psi)} \right) [L_5 Z_5 + G_5^*]\,, \\
\|\iota_6 A\| &\le A_0 + \left(\frac{\psi(1-\tau)T_{\min}^{\psi-1}}{AB(\tau)} + \frac{\tau T^{\tau+\psi-1}\Gamma(\psi+1)}{AB(\tau)\Gamma(\tau+\psi)} \right) [L_6 Z_6 + G_6^*]\,, \\
\|\iota_7 T_H\| &\le T_{H0} + \left(\frac{\psi(1-\tau)T_{\min}^{\psi-1}}{AB(\tau)} + \frac{\tau T^{\tau+\psi-1}\Gamma(\psi+1)}{AB(\tau)\Gamma(\tau+\psi)} \right) [L_7 Z_7 + G_7^*]\,. \qquad (21)
\end{aligned}$$

This implies $\iota D_{Z1} \subset D_{Z1}$.

Secondly, we show that ι is a contraction. Assume
$(S_H(t), S_{PREP}(t), E_H(t), E_{PEP}(t), I_H(t), A(t), T_H(t)) \in D_{Z1}$,
and
$(S_H^*(t), S_{PREP}^*(t), E_H^*(t), E_{PEP}^*(t), I_H^*(t), A^*(t), T_H^*(t)) \in D_{Z1}$.

We have

$$\begin{aligned}
&|(\iota_1 S_H)(t) - (\iota_1 S_H^*)(t)| \\
&\leq \frac{\psi t^{\psi-1}(1-\tau)}{AB(\tau)} \left|G_1(t, S_H(t)) - G_1(t, S_H^*(t))\right| \\
&\quad + \frac{\psi\tau}{AB(\tau)\Gamma(\tau)} \int_0^t s^{\psi-1}(t-s)^{\tau-1} \left|G_1(s, S_H(s)) - G_1(s, S_H^*(s))\right| ds, \\
&\leq \frac{\psi t^{\psi-1}(1-\tau)}{AB(\tau)} L_1 \Delta(t) + \frac{\psi\tau}{AB(\tau)\Gamma(\tau)} \int_0^t s^{\psi-1}(t-s)^{\tau-1} L_1 \Delta(s)\, ds, \\
&\leq \left(\frac{\psi(1-\tau)T_{\min}^{\psi-1}}{AB(\tau)} + \frac{\tau T^{\tau+\psi-1}\Gamma(\psi+1)}{\Gamma(\psi+\tau)} \right) \frac{L_1}{AB(\tau)} \|\Delta\|. \qquad (22)
\end{aligned}$$

Similarly, for $i = 2, 3, \ldots, 7$, we obtain

$$\begin{aligned}
&|(\iota_2 S_{PREP})(t) - (\iota_2 S_{PREP}^*)(t)| \\
&\quad \leq \left(\frac{\psi(1-\tau)T_{\min}^{\psi-1}}{AB(\tau)} + \frac{\tau T^{\tau+\psi-1}\Gamma(\psi+1)}{\Gamma(\psi+\tau)} \right) \frac{L_2}{AB(\tau)} \sum_j \left\|X_j - X_j^*\right\|, \\
&|(\iota_3 E_H)(t) - (\iota_3 E_H^*)(t)| \\
&\quad \leq \left(\frac{\psi(1-\tau)T_{\min}^{\psi-1}}{AB(\tau)} + \frac{\tau T^{\tau+\psi-1}\Gamma(\psi+1)}{\Gamma(\psi+\tau)} \right) \frac{L_3}{AB(\tau)} \sum_j \left\|X_j - X_j^*\right\|, \\
&|(\iota_4 E_{PEP})(t) - (\iota_4 E_{PEP}^*)(t)| \\
&\quad \leq \left(\frac{\psi(1-\tau)T_{\min}^{\psi-1}}{AB(\tau)} + \frac{\tau T^{\tau+\psi-1}\Gamma(\psi+1)}{\Gamma(\psi+\tau)} \right) \frac{L_4}{AB(\tau)} \sum_j \left\|X_j - X_j^*\right\|, \\
&|(\iota_5 I_H)(t) - (\iota_5 I_H^*)(t)| \\
&\quad \leq \left(\frac{\psi(1-\tau)T_{\min}^{\psi-1}}{AB(\tau)} + \frac{\tau T^{\tau+\psi-1}\Gamma(\psi+1)}{\Gamma(\psi+\tau)} \right) \frac{L_5}{AB(\tau)} \sum_j \left\|X_j - X_j^*\right\|, \\
&|(\iota_6 A)(t) - (\iota_6 A^*)(t)| \\
&\quad \leq \left(\frac{\psi(1-\tau)T_{\min}^{\psi-1}}{AB(\tau)} + \frac{\tau T^{\tau+\psi-1}\Gamma(\psi+1)}{\Gamma(\psi+\tau)} \right) \frac{L_6}{AB(\tau)} \sum_j \left\|X_j - X_j^*\right\|,
\end{aligned}$$

$$
\begin{aligned}
&|(\iota_7 T_H)(t) - (\iota_7 T_H^*)(t)| \\
&\leq \left(\frac{\psi(1-\tau)T_{\min}^{\psi-1}}{AB(\tau)} + \frac{\tau T^{\tau+\psi-1}\Gamma(\psi+1)}{\Gamma(\psi+\tau)} \right) \frac{L_7}{AB(\tau)} \sum_j \left\| X_j - X_j^* \right\|, \qquad (23)
\end{aligned}
$$

where

$$
\begin{aligned}
\sum_j \left\| X_j - X_j^* \right\| = &\|S_H - S_H^*\| + \|S_{PREP} - S_{PREP}^*\| \\
&+ \|E_H - E_H^*\| + \|E_{PEP} - E_{PEP}^*\| \\
&+ \|I_H - I_H^*\| + \|A - A^*\| + \|T_H - T_H^*\|.
\end{aligned}
$$

Since $\iota = (\iota_1, \iota_2, \iota_3, \iota_4, \iota_5, \iota_6, \iota_7)$ and $L_{\max} > 0$, we have

$$
\begin{aligned}
&\|\iota\left(t, S_H, S_{PREP}, E_H, E_{PEP}, I_H, A, T_H\right) \\
&-\iota\left(t, S_H^*, S_{PREP}^*, E_H^*, E_{PEP}^*, I_H^*, A^*, T_H^*\right)\| \\
&\leq \left(\frac{\psi(1-\tau)T_{\min}^{\psi-1}}{AB(\tau)} + \frac{\tau T^{\tau+\psi-1}\Gamma(\psi+1)}{\Gamma(\psi+\tau)} \right) \\
&\quad \cdot \frac{L_{\max}}{AB(\tau)} \begin{bmatrix} \|S_H - S_H^*\| + \|S_{PREP} - S_{PREP}^*\| + \|E_H - E_H^*\| \\ + \|E_{PEP} - E_{PEP}^*\| + \|I_H - I_H^*\| + \|A - A^*\| + \|T_H - T_H^*\| \end{bmatrix}.
\end{aligned}
$$

By the condition, ι is a contraction. By Lemma 2, the FF-HIV/AIDS model (8) has a unique solution.

The biological implication of this fractal-fractional fixed point theorem is that it guarantees a *unique* long-term trajectory for the HIV/AIDS epidemic under given initial conditions and intervention strategies. In real-world terms, this means that the future course of the epidemic—how many people will be susceptible, exposed, infected, or under treatment—is determined *unambiguously* by current population states and control measures (e.g., PrEP uptake, ART coverage, condom use). This uniqueness is critical for public health decision-making: Policymakers can trust that model predictions (such as the expected decline in new infections by 28% by 2033) are not ambiguous or dependent on arbitrary mathematical artifacts. It ensures that intervention planning—whether scaling up prophylaxis, improving treatment access, or enhancing behavioral prevention—will have a consistent, predictable impact on disease dynamics, thereby supporting reliable resource allocation and epidemic control in high-prevalence settings like South Africa. □

Theorem 3. Let $G \in X$ satisfy the assumptions (B_1) in Theorem 2 and (B_1). There exist constants $g_{i,j} > 0$, $i = 0, 1, \ldots, 6$, $j = 0, 1, \ldots, 6$, such that

$$
\begin{aligned}
&|G\left(S_H(t), S_{PREP}(t), E_H(t), E_{PEP}(t), I_H(t), A(t), T_H(t)\right)| \\
&\leq g_{0j} + g_{1j}\left|S_H(t)\right| + g_{2j}\left|S_{PREP}(t)\right| + g_{3j}\left|E_H(t)\right| \\
&\quad + g_{4j}\left|E_{PEP}(t)\right| + g_{5j}\left|I_H(t)\right| + g_{6j}\left|A(t)\right| + g_{7j}\left|T_H(t)\right|.
\end{aligned}
$$

If $\psi(1-\tau)T_{\min}^{\psi-1}L_{\max}AB(\tau) < 1$, then the HIV/AIDS model (1) has at least one solution.

Proof. We define a set

$$
D_{Z2} = \left\{ \begin{array}{l} (S_H(t), S_{PREP}(t), E_H(t), E_{PEP}(t), I_H(t), A(t), T_H(t)) \in X : \\ \|(S_H, S_{PREP}, E_H, E_{PEP}, I_H, A, T_H)\| \leq Z_2 \end{array} \right\}.
$$

Applying the model equations, we define two operators $(Q, P) : D_{Z2} \to X$, where $P = (P_1, P_2, P_3, P_4, P_5, P_6, P_7)$.

The operator Q is defined by

$$
\begin{aligned}
(Q_1, S_H)(t) &= S_H(0) + \frac{\psi t^{\psi-1}(1-\tau)G_1(t, S_H(t))}{AB(\tau)}, \\
(Q_2, S_{PREP})(t) &= S_{PREP}(0) + \frac{\psi t^{\psi-1}(1-\tau)G_2(t, S_{PREP}(t))}{AB(\tau)}, \\
(Q_3, E_H)(t) &= E_H(0) + \frac{\psi t^{\psi-1}(1-\tau)G_3(t, E_H(t))}{AB(\tau)}, \\
(Q_4, E_{PEP})(t) &= E_{PEP}(0) + \frac{\psi t^{\psi-1}(1-\tau)G_4(t, E_{PEP}(t))}{AB(\tau)}, \\
(Q_5, I_H)(t) &= I_H(0) + \frac{\psi t^{\psi-1}(1-\tau)G_5(t, I_H(t))}{AB(\tau)}, \\
(Q_6, A)(t) &= A(0) + \frac{\psi t^{\psi-1}(1-\tau)G_6(t, A(t))}{AB(\tau)}, \\
(Q_7, T_H)(t) &= T_H(0) + \frac{\psi t^{\psi-1}(1-\tau)G_7(t, T_H(t))}{AB(\tau)}.
\end{aligned} \tag{24}
$$

The operator P is defined by

$$
\begin{aligned}
(P_1, S_H)(t) &= \frac{\psi\tau}{AB(\tau)\Gamma(\tau)} \int_0^t s^{\psi-1}(t-s)^{\tau-1} G_1(s, S_H(s))\, ds, \\
(P_2, S_{PREP})(t) &= \frac{\psi\tau}{AB(\tau)\Gamma(\tau)} \int_0^t s^{\psi-1}(t-s)^{\tau-1} G_2(s, S_{PREP}(s))\, ds, \\
(P_3, E_H)(t) &= \frac{\psi\tau}{AB(\tau)\Gamma(\tau)} \int_0^t s^{\psi-1}(t-s)^{\tau-1} G_3(s, E_H(s))\, ds, \\
(P_4, E_{PEP})(t) &= \frac{\psi\tau}{AB(\tau)\Gamma(\tau)} \int_0^t s^{\psi-1}(t-s)^{\tau-1} G_4(s, E_{PEP}(s))\, ds, \\
(P_5, I_H)(t) &= \frac{\psi\tau}{AB(\tau)\Gamma(\tau)} \int_0^t s^{\psi-1}(t-s)^{\tau-1} G_5(s, I_H(s))\, ds,
\end{aligned}
$$

$$(P_6, A)(t) = \frac{\psi\tau}{AB(\tau)\Gamma(\tau)} \int_0^t s^{\psi-1}(t-s)^{\tau-1} G_6(s, A(s))\, ds,$$
$$(P_7, T_H)(t) = \frac{\psi\tau}{AB(\tau)\Gamma(\tau)} \int_0^t s^{\psi-1}(t-s)^{\tau-1} G_7(s, T_H(s))\, ds. \tag{25}$$

Using (B_1) in Theorem 2, for any

$$(S_H(t), S_{PREP}(t), E_H(t), E_{PEP}(t), I_H(t), A(t), T_H(t)) \in D_{Z2}$$

and

$$(S_H^*(t), S_{PREP}^*(t), E_H^*(t), E_{PEP}^*(t), I_H^*(t), A^*(t), T_H^*(t)) \in D_{Z2},$$

from the above, with $L_{\max}$, it follows that

$$\|Q_1 S_H - Q_1 S_H^*\| \leq \frac{\psi(1-\tau)T_{\min}^{\psi-1}}{AB(\tau)} \sup |G_1(t, S_H(t)) - G_1(t, S_H^*(t))|,$$
$$\begin{aligned}
&\|Q_1 S_H - Q_1 S_H^*\| \\
&\leq \frac{\psi(1-\tau)T_{\min}^{\psi-1}}{AB(\tau)} L_1 \left(\|S_H - S_H^*\| + \|S_{PREP} - S_{PREP}^*\| + \|E_H - E_H^*\| \right. \\
&\quad \left. + \|E_{PEP} - E_{PEP}^*\| + \|I_H - I_H^*\| + \|A - A^*\| + \|T_H - T_H^*\|\right), \\
&\|Q_2 S_{PREP} - Q_2 S_{PREP}^*\| \\
&\leq \frac{\psi(1-\tau)T_{\min}^{\psi-1}}{AB(\tau)} L_2 \left(\|S_H - S_H^*\| + \|S_{PREP} - S_{PREP}^*\| + \|E_H - E_H^*\| \right. \\
&\quad \left. + \|E_{PEP} - E_{PEP}^*\| + \|I_H - I_H^*\| + \|A - A^*\| + \|T_H - T_H^*\|\right), \\
&\|Q_3 E_H - Q_3 E_H^*\| \\
&\leq \frac{\psi(1-\tau)T_{\min}^{\psi-1}}{AB(\tau)} L_3 \left(\|S_H - S_H^*\| + \|S_{PREP} - S_{PREP}^*\| + \|E_H - E_H^*\| \right. \\
&\quad \left. + \|E_{PEP} - E_{PEP}^*\| + \|I_H - I_H^*\| + \|A - A^*\| + \|T_H - T_H^*\|\right), \\
&\|Q_4 E_{PEP} - Q_4 E_{PEP}^*\| \\
&\leq \frac{\psi(1-\tau)T_{\min}^{\psi-1}}{AB(\tau)} L_4 \left(\|S_H - S_H^*\| + \|S_{PREP} - S_{PREP}^*\| + \|E_H - E_H^*\| \right. \\
&\quad \left. + \|E_{PEP} - E_{PEP}^*\| + \|I_H - I_H^*\| + \|A - A^*\| + \|T_H - T_H^*\|\right), \\
&\|Q_5 I_H - Q_5 I_H^*\| \\
&\leq \frac{\psi(1-\tau)T_{\min}^{\psi-1}}{AB(\tau)} L_5 \left(\|S_H - S_H^*\| + \|S_{PREP} - S_{PREP}^*\| + \|E_H - E_H^*\| \right. \\
&\quad \left. + \|E_{PEP} - E_{PEP}^*\| + \|I_H - I_H^*\| + \|A - A^*\| + \|T_H - T_H^*\|\right),
\end{aligned}$$

$$
\begin{aligned}
&\|Q_6 A - Q_6 A^*\| \\
&\leq \frac{\psi(1-\tau)T_{\min}^{\psi-1}}{AB(\tau)} L_6 \left(\|S_H - S_H^*\| + \|S_{PREP} - S_{PREP}^*\| + \|E_H - E_H^*\|\right. \\
&\quad \left. + \|E_{PEP} - E_{PEP}^*\| + \|I_H - I_H^*\| + \|A - A^*\| + \|T_H - T_H^*\|\right), \\
&\|Q_7 T_H - Q_7 T_H^*\| \\
&\leq \frac{\psi(1-\tau)T_{\min}^{\psi-1}}{AB(\tau)} L_7 \left(\|S_H - S_H^*\| + \|S_{PREP} - S_{PREP}^*\| + \|E_H - E_H^*\|\right. \\
&\quad \left. + \|E_{PEP} - E_{PEP}^*\| + \|I_H - I_H^*\| + \|A - A^*\| + \|T_H - T_H^*\|\right). \qquad (26)
\end{aligned}
$$

Thus, P is bounded and equicontinuous, ensuring the HIV/AIDS model has at least one solution under the given conditions.

The biological implication of this fractal-fractional existence theorem is that, regardless of whether the disease dynamics are highly nonlinear or intervention effects are complex, *at least one realistic disease trajectory exists* that is consistent with the model's assumptions and observed data. In practical terms, this means that the epidemic will follow *some* biologically plausible path over time—whether it declines due to effective interventions (e.g., high ART coverage, PrEP use) or persists at endemic levels. This guarantees that the model is mathematically sound and capable of producing valid simulations, even when strong contraction conditions (required for uniqueness) are not met. For public health, this result underpins the reliability of numerical forecasts (such as the projected 28% reduction in new infections by 2033) and ensures that policy simulations—testing "what-if" scenarios like increased prophylaxis or treatment access—are grounded in a solution that respects real-world constraints and disease biology. □

4.1 The endemic equilibrium point of the HIV/AIDS model

The endemic equilibrium point refers to a state where HIV/AIDS persists in the population at constant levels.

Theorem 4. The endemic equilibrium point of the HIV/AIDS model in (1) is stable whenever $R_{0H} > 1$ and unstable if $R_{0H} < 1$.

Proof. At the endemic equilibrium point,

$$
\frac{dS_H}{dt} = \frac{dS_{PREP}}{dt} = \frac{dE}{dt} = \frac{dE_{PEP}}{dt} = \frac{dI}{dt} = \frac{dI}{dt} = \frac{dA}{dt} = \frac{dT}{dt} = 0.
$$

Let the endemic equilibrium point of the model (1) be
$\widehat{\varepsilon} = \left(S_H^*, S_{PREP}^*, E_H^*, E_{PEP}^*, I_H^*, A^*, T_H^*\right)$.

By setting the right-hand side of the HIV/AIDS model equations in (1) to zero(0) and solving for each compartments, we obtain

$$\begin{aligned}
S_H^* &= \frac{\Lambda_H}{\lambda_H^* + Z_1},\\
S_{PREP}^* &= \frac{\omega_H\,\Lambda_H}{(\lambda_H^* + Z_1)\,(-\lambda_H^*\,\varepsilon_1 + \theta_H + \lambda_H^*)},\\
E_H^* &= \frac{\lambda_H^*\,\Lambda_H\,\left(-\lambda_H^*\,\varepsilon_1 + \theta_H + Z_2 + \lambda_H^*\right)}{(\lambda_H^* + Z_1)\,(-\lambda_H^*\,\varepsilon_1 + \theta_H + \lambda_H^*)\,P_1},\\
E_{PEP}^* &= \frac{\lambda_H^*\,\Lambda_H\,\left(-\lambda_H^*\,\varepsilon_1 + \theta_H + Z_2 + \lambda_H^*\right)v_{21}}{(\lambda_H^* + Z_1)\,(-\lambda_H^*\,\varepsilon_1 + \theta_H + \lambda_H^*)\,P_1\,P_2},\\
I_H^* &= \frac{(-\lambda_H^*\,\varepsilon_1 + \theta_H + Z_2 + \lambda_H^*)\,\lambda_H^*\,P_4\,\left(P_2\,v_{31} + v_{21}\,v_{32}\right)\Lambda_H\,P_5}{(\lambda_H^* + Z_1)\,(-\lambda_H^*\,\varepsilon_1 + \theta_H + \lambda_H^*)\,P_1\,P_2\,\left(P_3\,P_4\,P_5 - P_4\,\chi\,\theta_1 - \chi\,\theta_2\,\rho_1\right)},\\
A^* &= \frac{(-\lambda_H^*\,\varepsilon_1 + \theta_H + Z_2 + \lambda_H^*)\,\lambda_H^*\,\left(P_2\,v_{31} + v_{21}\,v_{32}\right)\Lambda_H\,P_5\,\rho_1}{(\lambda_H^* + Z_1)\,(-\lambda_H^*\,\varepsilon_1 + \theta_H + \lambda_H^*)\,P_1\,P_2\,\left(P_3\,P_4\,P_5 - P_4\,\chi\,\theta_1 - \chi\,\theta_2\,\rho_1\right)},\\
T_H^* &= \frac{(P_4\,\theta_1 + \theta_2\,\rho_1)\,(-\lambda_H^*\,\varepsilon_1 + \theta_H + Z_2 + \lambda_H^*)\,\lambda_H^*\,\left(P_2\,v_{31} + v_{21}\,v_{32}\right)\Lambda_H}{(\lambda_H^* + Z_1)\,(-\lambda_H^*\,\varepsilon_1 + \theta_H + \lambda_H)\,P_1\,P_2\,\left(P_3\,P_4\,P_5 - P_4\,\chi\,\theta_1 - \chi\,\theta_2\,\rho_1\right)}.
\end{aligned} \tag{27}$$

Here
$v_{21} = \theta\sigma_1,\ v_{31} = (1-\theta)\,\sigma_1,\ v_{32} = (1-\varepsilon_2)\,\sigma_2,$
$P_1 = (\sigma_1 + \theta_H), P_2 = ((1-\varepsilon_2)\,\sigma_2 + \theta_H), P_3 = (\theta_1 + \rho_1 + \delta_I + \theta_H),$
$P_4 = (\theta_2 + \delta_A + \theta_H), P_5 = (\chi + \Theta\delta_T + \theta_H),\ Z_1 = (\omega_H + \theta_H),$
$Z_2 = ((1-\varepsilon_1)\,\omega_H + \theta_H).$

Further simplification of the endemic equilibrium point of the model as presented in equation (27) yields the final endemic equilibrium point.

Substituting the endemic equilibrium point of the HIV/AIDS model $\widehat{\varepsilon}$ into its force of infection
$\lambda_H^* = \frac{(1-\varsigma\Psi)\gamma\gamma_H\left(I_H^* + A^* + \eta T_H^*\right)}{N^*}$, we obtain

$$\lambda_H^*\left(\widehat{C_1}\,{\lambda_H^*}^4 + \widehat{C_2}\,{\lambda_H^*}^3 + \widehat{C_3}\,{\lambda_H^*}^2 + \widehat{C_4}\,\lambda_H^* + \widehat{C_5}\right) = 0. \tag{28}$$

But at the endemic equilibrium ($\lambda_H \neq 0$), hence

$$\widehat{C_1}\,{\lambda_H^*}^4 + \widehat{C_2}\,{\lambda_H^*}^3 + \widehat{C_3}\,{\lambda_H^*}^2 + \widehat{C_4}\,\lambda_H^* + \widehat{C_5} = 0, \tag{29}$$

where

$$\begin{aligned}\widehat{C_1} =&\Lambda_H\ ((-P_3\,P_5+\chi\,\theta_1)\,P_4+\chi\,\theta_2\,\rho_1)\,P_1\,P_2\ (\varepsilon_1-1)^2\\&\times((((-P_3-v_{31})\,P_5+\theta_1\ (\chi-v_{31}))\,P_2\\&+((-P_3-v_{32})\,P_5+\theta_1\ (\chi-v_{32}))\,v_{21})\,P_4\\&+((-v_{31}\,P_5+\theta_2\ (\chi-v_{31}))\,P_2+v_{21}\ (-v_{32}\,P_5+\theta_2\ (\chi-v_{32})))\,\rho_1)\,,\end{aligned}$$

$$\begin{aligned}\widehat{C_2} =&-((-P_3\,P_5+\chi\,\theta_1)\,P_4+\chi\,\theta_2\,\rho_1)\,P_1\,(\varepsilon_1-1)\,\Lambda_H\\&\times[(((\gamma\,v_{31}\,(\Psi\,\varsigma-1)\,\gamma_H+v_{31}\,Z_1+P_3\,(P_1+Z_1))\,\varepsilon_1-\gamma\,v_{31}(\Psi\,\varsigma-1)\gamma_H\\&+(-Z_2-2\theta_H-Z_1)v_{31}\ -P_3(Z_2+2\theta_H+P_1+Z_1))\,P_5\\&+((\gamma\,v_{31}\,\eta\,(\Psi\,\varsigma-1)\,\gamma_H+v_{31}\,Z_1-\chi(P_1+Z_1))\,\varepsilon_1-\gamma\,v_{31}\,\eta\,(\Psi\,\varsigma-1)\,\gamma_H\\&\quad+(-Z_2-2\theta_H-Z_1)v_{31}+\chi(Z_2+2\theta_H+P_1+Z_1))\,\theta_1)\,P_2\\&+v_{21}\,[((\gamma\,v_{32}\,(\Psi\,\varsigma-1)\gamma_H+Z_1(v_{32}+P_3))\,\varepsilon_1\\&\quad-\gamma\,v_{32}\,(\Psi\,\varsigma-1)\gamma_H-(v_{32}+P_3)(Z_2+2\theta_H+Z_1))\,P_5\\&\quad+((\gamma\,v_{32}\,\eta\,(\Psi\,\varsigma-1)\,\gamma_H+Z_1(v_{32}-\chi))\,\varepsilon_1\\&\quad-\gamma\,v_{32}\,\eta\,(\Psi\,\varsigma-1)\,\gamma_H-(v_{32}-\chi)(Z_2+2\theta_H+Z_1))\,\theta_1]\,P_4\\&+[((\gamma(\Psi\,\varsigma-1)\gamma_H+Z_1)\,\varepsilon_1\\&\quad+(-\Psi\,\varsigma+1)\gamma\,\gamma_H-Z_2-2\theta_H-Z_1)\,v_{31}\,P_5\\&\quad+\theta_2\ ((\gamma\,v_{31}\,\eta\,(\Psi\,\varsigma-1)\gamma_H+v_{31}Z_1-\chi(P_1+Z_1))\,\varepsilon_1\\&\quad-\gamma\,v_{31}\,\eta\,(\Psi\,\varsigma-1)\,\gamma_H+(-Z_2-2\theta_H-Z_1)v_{31}\\&\quad+\chi(Z_2+2\theta_H+P_1+Z_1))]\,P_2+(((\gamma(\Psi\,\varsigma-1)\gamma_H+Z_1)\,\varepsilon_1\\&+(-\Psi\,\varsigma+1)\gamma\,\gamma_H-Z_2-2\theta_H-Z_1)\,v_{32}\,P_5\\&+((\gamma\,v_{32}\,\eta\,(\Psi\,\varsigma-1)\,\gamma_H+Z_1(v_{32}-\chi))\,\varepsilon_1\\&-\gamma\,v_{32}\,\eta\,(\Psi\,\varsigma-1)\,\gamma_H-(v_{32}-\chi)(Z_2+2\theta_H+Z_1))\,\theta_2)\,v_{21})\,\rho_1\Big]P_2,\end{aligned}$$

$$\widehat{C_3}=\Big[(\mathcal{A}_1+\rho_1\mathcal{A}_2+\mathcal{A}_3+\rho_1\mathcal{A}_4)\,v_{21}\Big]\,((-P_3P_5+\chi\theta_1)\,P_4+\chi\theta_2\rho_1)\,P_1\Lambda_HP_2,$$

where

$$\begin{aligned}\mathcal{A}_1=&-(\varepsilon_1-1)\cdot\Big[\gamma v_{31}(\varepsilon_1-1)(\eta\theta_1+P_5)(\Psi\varsigma-1)\gamma_H\\&-P_1(-P_3P_5+\chi\theta_1)\varepsilon_1+\mathcal{X}_1-\theta_1\mathcal{Y}_1\Big]Z_1\\&+\gamma v_{31}(\varepsilon_1-1)(\eta\theta_1+P_5)(Z_2+2\theta_H)(\Psi\varsigma-1)\gamma_H\end{aligned}$$

$$- 2P_1(-P_3P_5 + \chi\theta_1)(\theta_H + \frac{\omega_H}{2})\varepsilon_1 + \mathcal{X}_2 - \theta_1\mathcal{Y}_2\Big)P_4,$$

$$\begin{aligned}\mathcal{A}_2 = &- (\varepsilon_1 - 1)\cdot\Big[\gamma v_{31}(\varepsilon_1 - 1)(\eta\theta_2 + P_5)(\Psi\varsigma - 1)\gamma_H \\ &- \theta_2\chi\varepsilon_1 P_1 - v_{31}(Z_2 + 2\theta_H)P_5 - \theta_2\mathcal{Y}_1\Big]Z_1 \\ &+ \gamma v_{31}(\varepsilon_1 - 1)(\eta\theta_2 + P_5)(Z_2 + 2\theta_H)(\Psi\varsigma - 1)\gamma_H \\ &- 2\theta_2\chi P_1(\theta_H + \frac{\omega_H}{2})\varepsilon_1 - v_{31}\theta_H(Z_2 + \theta_H)P_5 - \theta_2\mathcal{Y}_2\Big),\end{aligned}$$

$$\begin{aligned}\mathcal{A}_3 = &- (\varepsilon_1 - 1)\cdot\Big[\gamma v_{32}(\varepsilon_1 - 1)(\eta\theta_1 + P_5)(\Psi\varsigma - 1)\gamma_H \\ &- ((v_{32} + P_3)P_5 + \theta_1(v_{32} - \chi))\,(Z_2 + 2\theta_H)\Big]Z_1 \\ &+ \gamma v_{32}(\varepsilon_1 - 1)(\eta\theta_1 + P_5)(Z_2 + 2\theta_H)(\Psi\varsigma - 1)\gamma_H \\ &- \theta_H(Z_2 + \theta_H)\,((v_{32} + P_3)P_5 + \theta_1(v_{32} - \chi))\Big)P_4,\end{aligned}$$

$$\begin{aligned}\mathcal{A}_4 = &- (\varepsilon_1 - 1)\cdot\Big[\gamma v_{32}(\varepsilon_1 - 1)(\eta\theta_2 + P_5)(\Psi\varsigma - 1)\gamma_H \\ &- (Z_2 + 2\theta_H)\,(v_{32}P_5 + \theta_2(v_{32} - \chi))\Big]Z_1 \\ &+ \gamma v_{32}(\varepsilon_1 - 1)(\eta\theta_2 + P_5)(Z_2 + 2\theta_H)(\Psi\varsigma - 1)\gamma_H \\ &- \theta_H(Z_2 + \theta_H)\,(v_{32}P_5 + \theta_2(v_{32} - \chi))\Big),\end{aligned}$$

$$\begin{aligned}\mathcal{X}_1 &= (-2v_{31} - 2P_3)\,\theta_H - Z_2v_{31} - P_3(Z_2 + P_1), \\ \mathcal{Y}_1 &= (2v_{31} - 2\chi)\,\theta_H + Z_2v_{31} - \chi(Z_2 + P_1), \\ \mathcal{X}_2 &= (-P_3 - v_{31})\,\theta_H^2 + (-Z_2v_{31} - P_3(Z_2 + 2P_1))\,\theta_H - \omega_H P_1P_3, \\ \mathcal{Y}_2 &= (v_{31} - \chi)\theta_H^2 + (Z_2v_{31} - \chi(Z_2 + 2P_1))\,\theta_H - \chi\omega_H P_1,\end{aligned}$$

$$\begin{aligned}\widehat{C_4} = &- \Bigg(\Big[\Big(\big((v_{31} + P_3)P_5 + \theta_1(v_{31} - \chi)\big)P_4 + \rho_1\big(v_{31}P_5 + \theta_2(v_{31} - \chi)\big)\Big)P_2 \\ &+ v_{21}\Big(\big((v_{32} + P_3)P_5 + \theta_1(v_{32} - \chi)\big)P_4 + \rho_1\big(v_{32}P_5 + \theta_2(v_{32} - \chi)\big)\Big)\Big]Z_1 \\ &+ (P_2v_{31} + v_{21}v_{32})\gamma\Big((\eta\theta_1 + P_5)P_4 + \rho_1(\eta\theta_2 + P_5)\Big)(\Psi\varsigma - 1)\gamma_H \\ &- \Big((-P_3P_5 + \chi\theta_1)P_4 + \chi\theta_2\rho_1\Big)P_1P_2\Big)\theta_H^2 \\ &+ \Bigg[- 2(P_2v_{31} + v_{21}v_{32})\gamma(\varepsilon_1 - 1)\Big((\eta\theta_1 + P_5)P_4 + \rho_1(\eta\theta_2 + P_5)\Big)(\Psi\varsigma - 1)\gamma_H \\ &+ \Big(\Big(\big((v_{31} + P_3)Z_2 - 2P_1P_3(\varepsilon_1 - 1)\big)P_5 + \theta_1\big((v_{31} - \chi)Z_2 + 2\chi P_1(\varepsilon_1 - 1)\big)\Big)P_4\end{aligned}$$

$$
\begin{aligned}
&+\Big(Z_2 v_{31} P_5+\theta_2\big((v_{31}-\chi)Z_2+2\chi P_1(\varepsilon_1-1)\big)\Big)\rho_1\Big)P_2\\
&+Z_2 v_{21}\Big(\big((v_{32}+P_3)P_5+\theta_1(v_{32}-\chi)\big)P_4+\rho_1\big(v_{32}P_5+\theta_2(v_{32}-\chi)\big)\Big)\Big]Z_1\\
&+(P_2 v_{31}+v_{21}v_{32})\gamma Z_2\Big((\eta\theta_1+P_5)P_4+\rho_1(\eta\theta_2+P_5)\Big)(\Psi\varsigma-1)\gamma_H\\
&-\Big((-P_3P_5+\chi\theta_1)P_4+\chi\theta_2\rho_1\Big)P_1\omega_H P_2\Big)\theta_H\\
&-(\varepsilon_1-1)Z_1\Big[(P_2v_{31}+v_{21}v_{32})\gamma Z_2\Big((\eta\theta_1+P_5)P_4+\rho_1(\eta\theta_2+P_5)\Big)(\Psi\varsigma-1)\gamma_H\\
&-\Big((-P_3P_5+\chi\theta_1)P_4+\chi\theta_2\rho_1\Big)P_1\omega_H P_2\Big]\Big((-P_3P_5+\chi\theta_1)P_4+\chi\theta_2\rho_1\Big)P_1\Lambda_H P_2,
\end{aligned}
$$

$$
\begin{aligned}
\widehat{C_5} =&Z_1\,\theta_H\,\Lambda_H\,P_1\,P_2\,\left(P_3\,P_4\,P_5-P_4\,\chi\,\theta_1-\chi\,\theta_2\,\rho_1\right)\\
&\times\left(\left(\left(P_2\,v_{31}+v_{21}\,v_{32}\right)\left(\left(\eta\,\theta_1+P_5\right)P_4+\rho_1\,\left(\eta\,\theta_2+P_5\right)\right)\left(\Psi\,\varsigma-1\right)\gamma\,\gamma_H\right.\right.\\
&-P_1\,\left(\left(-P_3\,P_5+\chi\,\theta_1\right)P_4+\chi\,\theta_2\,\rho_1\right)P_2\Big)\,\theta_H\\
&-P_1\,\left(\left(-P_3\,P_5+\chi\,\theta_1\right)P_4+\chi\,\theta_2\,\rho_1\right)P_2\,\omega_H\Big)\\
&+{Z_1}^2\Lambda_H\,\left(\theta_H\left(P_1\,P_2\,\left(P_3\,P_4\,P_5-P_4\,\chi\,\theta_1-\chi\,\theta_2\,\rho_1\right)\right)\right)^2\left(1-R_{0H}\right).
\end{aligned}
$$

The components of the endemic equilibrium point (EEP) are determined by solving for λ_H^* from the polynomial equation (29) and substituting its positive values into the expressions given in (27). Moreover, based on the coefficients $\widehat{C_i}$ for $i=1,2,3,\ldots,5$, it is evident that $\widehat{C_1}$ is always positive, while $\widehat{C_5}$ is positive when $R_{0H}<1$ and negative when $R_{0H}>1$. From this, we derive the following results:

Theorem 5. The HIV/AIDS model (1) has

1. four or two endemic equilibria if $\widehat{C_2}<0,\widehat{C_3}>0,\widehat{C_4}<0$ and $R_{0H}<1$
2. four or two endemic equilibria if $\widehat{C_2}<0,\widehat{C_3}<0,\widehat{C_4}>0$ and $R_{0H}<1$
3. no endemic equilibrium otherwise if $R_{0H}<1$.

Items (1)–(3) of Theorem 5 indicate the potential occurrence of backward bifurcation in the HIV/AIDS model (1) when $R_{0H}<1$. The presence of backward bifurcation implies that the conventional condition of having the basic reproduction number R_{0H} less than one, while necessary, is no longer sufficient to ensure the elimination of the disease from the population.

The biological implication of this fractal-fractional equilibrium analysis is profound for HIV control: When $R_{0H}>1$, the disease settles into a stable, persistent state—meaning HIV will

remain in the population at a constant level unless interventions are dramatically strengthened. Conversely, when $R_{0H} < 1$, the disease-free state is stable, and elimination is possible—but the risk of *backward bifurcation* warns that simply reducing R_{0H} below 1 may not be enough. In real-world terms, this means that even with moderate success in interventions (e.g., partial PrEP coverage, inconsistent condom use, or incomplete ART access), HIV can persist at low but stable levels due to residual transmission chains, behavioral heterogeneity, or treatment dropout. This phenomenon explains why some regions struggle to eliminate HIV despite $R_{0H} < 1$. The model thus urges policymakers to push R_{0H} *significantly below 1* and sustain high intervention synergy (condoms + PrEP + ART) to avoid being trapped in a low-level endemic trap—critical insight for achieving the UNAIDS 95-95-95 targets and ending AIDS as a public health threat by 2030. □

4.2 Global and asymptotic stability of HIV/AIDS at endemic equilibrium

The purpose of this work is to demonstrate the global asymptotic stability of HIV/AIDS endemic equilibrium points $\hat{\varepsilon}$.

Lemma 4. If $R_{0H} > 1$, then additional conditions allow for the proof of global asymptotic stability at the endemic equilibrium for system (1).

Proof. Let the Lyapunov function $U = U(S_H, S_{PREP}, E_H, E_{PEP}, I_H, A, T_H)$ be defined as follows:

$$\begin{aligned} U =& U_1\left(S_H - S_H^* - S_H^* \ln\left(\frac{S_H^*}{S_H}\right)\right) \\ &+ U_2\left(S_{PREP} - S_{PREP}^* - S_{PREP}^* \ln\left(\frac{S_{PREP}^*}{S_{PREP}}\right)\right) \\ &+ U_3\left(E_H - E_H^* - E_H^* \ln\left(\frac{E_H^*}{E_H}\right)\right) \\ &+ U_4\left(E_{PEP} - E_{PEP}^* - E_{PEP}^* \ln\left(\frac{E_{PEP}^*}{E_{PEP}}\right)\right) \\ &+ U_5\left(I_H - I_H^* - I_H^* \ln\left(\frac{I_H^*}{I_H}\right)\right) + U_6\left(A - A^* - A^* \ln\left(\frac{A^*}{A}\right)\right) \\ &+ U_7\left(T_H - T_H^* - T_H^* \ln\left(\frac{T_H^*}{T_H}\right)\right). \end{aligned} \tag{30}$$

By differentiating the Lyapunov function U with respect to time t along the positive system solutions of (30), we obtain

$$\begin{aligned}\frac{dU}{dt} =& U_1\left(1-\frac{S_H^*}{S_H}\right)\frac{dS_H}{dt}+U_2\left(1-\frac{S_{PREP}^*}{S_{PREP}}\right)\frac{dS_{PREP}}{dt}\\ &+U_3\left(1-\frac{E_H^*}{E_H}\right)\frac{dE_H}{dt}+U_4\left(1-\frac{E_{PEP}^*}{E_{PEP}}\right)\frac{dE_{PEP}}{dt}\\ &+U_5\left(1-\frac{I_H^*}{I_H}\right)\frac{dI_H}{dt}+U_6\left(1-\frac{A^*}{A}\right)\frac{dA}{dt}\\ &+U_7\left(1-\frac{T_H^*}{T_H}\right)\frac{dT_H}{dt}.\end{aligned} \tag{31}$$

Substituting the derivatives into the above, we have

$$\begin{aligned}\frac{dU}{dt} =& U_1\left(1-\frac{S_H^*}{S_H}\right)(\Lambda-\lambda_H S_H-Z_1 S_H)\\ &+U_2\left(1-\frac{S_{PREP}^*}{S_{PREP}}\right)(\omega_H S_H-(1-\varepsilon_1)\lambda_H S_{PREP}-Z_2 S_{PREP})\\ &+U_3\left(1-\frac{E_H^*}{E_H}\right)(\lambda_H S_H+(1-\varepsilon_1)\lambda_H S_{PREP}-P_1 E_H)\\ &+U_4\left(1-\frac{E_{PEP}^*}{E_{PEP}}\right)(v_{21}E_H-P_2 E_{PEP})\\ &+U_5\left(1-\frac{I_H^*}{I_H}\right)(v_{31}E_H+v_{32}E_{PEP}-P_3 I_H+\chi T_H)\\ &+U_6\left(1-\frac{A^*}{A}\right)(\rho_1 I_H-P_4 A)\\ &+U_7\left(1-\frac{T_H^*}{T_H}\right)(\theta_1 I_H+\theta_2 A-P_5 T_H),\end{aligned} \tag{32}$$

where the parameters are defined as follows:

$$\begin{aligned}&Z_1=\omega_H+\theta_H, Z_2=(1-\varepsilon_1)\lambda_H+\theta_H, P_1=\sigma_1+\theta_H,\\ &P_2=(1-\varepsilon_2)\sigma_2+\theta_H, P_3=\theta_1+\rho_1+\delta_I+\theta_H, P_4=\theta_2+\delta_A+\theta_H,\\ &P_5=\chi+\Theta\delta_T+\theta_H.\end{aligned} \tag{33}$$

At the endemic equilibrium point, we have

$$
\begin{aligned}
\Lambda &= \lambda_H S_H^* + Z_1 S_H^*, \\
P_1 &= \frac{\lambda_H S_H^* + (1-\varepsilon_1)\lambda_H S_{PREP}^*}{E_H^*}, \\
P_2 &= \frac{v_{21} E_H^*}{E_{PEP}^*}, \\
P_3 &= \frac{v_{31} E_H^* + v_{32} E_{PEP}^* + \chi T_H^*}{I_H^*}, \\
P_4 &= \frac{\rho_1 I_H^*}{A^*}, \\
P_5 &= \frac{\theta_1 I_H^* + \theta_2 A^*}{T_H^*}.
\end{aligned} \tag{34}
$$

Substituting $\Lambda, Z_1, P_1, P_2, P_3, P_4, P_5$ into the expression for $\frac{dU}{dt}$, we have

$$
\begin{aligned}
\frac{dU}{dt} =& U_1 \left(1 - \frac{S_H^*}{S_H}\right)\left(\lambda_H S_H^* + Z_1 S_H^* - (\lambda_H S_H + Z_1 S_H)\right) \\
&+ U_2 \left(1 - \frac{S_{PREP}^*}{S_{PREP}}\right)\left(\omega_H S_H - \frac{\omega_H S_H^*}{S_{PREP}^*} S_{PREP}\right) \\
&+ U_3 \left(1 - \frac{E_H^*}{E_H}\right)\left(\lambda_H S_H + (1-\varepsilon_1)\lambda_H S_{PREP}\right. \\
&\quad \left. - \frac{\lambda_H S_H^* + (1-\varepsilon_1)\lambda_H S_{PREP}^*}{E_H^*} E_H\right) \\
&+ U_4 \left(1 - \frac{E_{PEP}^*}{E_{PEP}}\right)\left(v_{21} E_H - \frac{v_{21} E_H^*}{E_{PEP}^*} E_{PEP}\right) \\
&+ U_5 \left(1 - \frac{I_H^*}{I_H}\right)\left(v_{31} E_H + v_{32} E_{PEP} + \chi T_H\right. \\
&\quad \left. - \frac{v_{31} E_H^* + v_{32} E_{PEP}^* + \chi T_H^*}{I_H^*} I_H\right) \\
&+ U_6 \left(1 - \frac{A^*}{A}\right)\left(\rho_1 I_H - \frac{\rho_1 I_H^*}{A^*} A\right) \\
&+ U_7 \left(1 - \frac{T_H^*}{T_H}\right)\left(\theta_1 I_H + \theta_2 A - \frac{\theta_1 I_H^* + \theta_2 A^*}{T_H^*} T_H\right).
\end{aligned} \tag{35}
$$

We obtain after performing expansion and collection of the positive and negative terms: $\frac{dU}{dt} = A - B$, where

$$
\begin{aligned}
A =& \lambda_H S_H^* U_1 + Z_1 S_H^* U_1 + \frac{\lambda_H S_H^{*2} U_1}{S_H} + \frac{Z_1 S_H^{*2} U_1}{S_H} \\
&+ \lambda_H S_H U_3 + (1-\varepsilon_1)\lambda_H S_{PREP} U_3 + \lambda_H S_H^* U_3 + (1-\varepsilon_1)\lambda_H S_{PREP}^* U_3,
\end{aligned} \tag{36}
$$

and

$$\begin{aligned} B =&\lambda_H S_H^* U_1 + Z_1 S_H^* U_1 + Z_1 S_H^* U_1 + \frac{\lambda_H S_H^{*2} U_1}{S_H} + \frac{Z_1 S_H^2 U_1}{S_H} \\ &+ \frac{\lambda_H S_H^{*2} E_H U_3}{E_H^*} + \frac{\lambda_H S_H E_H^* U_3}{E_H} + (1-\varepsilon_1)\frac{\lambda_H S_{PREP} E_H^* U_3}{E_H} \\ &+ \frac{U_5 v_{31} E_H^* I_H}{I_H^*} + \frac{U_5 v_{31} E_H I_H^*}{I_H} + \frac{U_5 v_{32} E_{PEP}^* I_H}{I_H^*} + \frac{U_5 v_{32} E_{PEP} I_H^*}{I_H}. \end{aligned} \tag{37}$$

Hence, since $B < A$, we have $\frac{dU}{dt} \leq 0$ with $\frac{dU}{dt} = 0$ if and only if
$S_H = S_H^*, S_{PREP} = S_{PREP}^*, E_H = E_H^*, E_{PEP} = E_{PEP}^*, I_H = I_H^*, A = A^*, T_H = T_H^*$.
Therefore, the largest compact invariant set is a singleton set $\{E_H^*\}$ that contains the endemic equilibrium point of the system (1). The stability analysis demonstrates that the system (1) $\hat{\varepsilon}$ is globally and asymptotically stable in accordance with La Salle's invariant principle as indicated in La Salle [32]:
$\left\{(S_H^*, S_{PREP}^*, E_H^*, E_{PEP}^*, I_H^*, A^*, T_H^*) \in \Omega_H : \frac{dU}{dt} = 0\right\}$.

The biological implication of this global asymptotic stability result is that, when $R_{0H} > 1$, the HIV epidemic will inevitably converge to a persistent, self-sustaining level—regardless of initial conditions (e.g., a small outbreak, a major surge, or partial intervention rollout). In real-world terms, this means that once transmission exceeds the critical threshold, HIV becomes endemic and irreversible without drastic, sustained intervention. The population will settle into a predictable, long-term state with fixed proportions of infected, treated, and at-risk individuals. This result is critical for public health planning: It confirms that half-measures will not work—PrEP, ART, and condom promotion must be scaled aggressively and maintained indefinitely to push R_{0H} below 1 and prevent convergence to this stable endemic trap. For policymakers, this underscores the urgency of achieving and sustaining the UNAIDS 95-95-95 targets; any lapse risks locking the epidemic into a costly, lifelong burden on healthcare systems and communities. □

4.3 Numerical schemes for the fractal-fractional HIV/AIDS model

The second-order Adams–Bashforth algorithm will be used to create numerical solutions for the HIV/AIDS model (1).
We rewrite the integral equations, at $t = t_{n+1}$, this yields

$$
\begin{aligned}
S_H(t_{n+1}) =& S_{H0} + \psi(1-\tau)t_n^{\psi-1}G_1(t_n, S_H(t_n)) \\
&+ \frac{\tau\psi}{AB(\tau)\Gamma(\tau)}\int_0^{t_{n+1}}(t_{n+1}-s)^{\tau-1}S_H^{\psi-1}G_1(s, S_H(s))\,ds, \\
S_{PREP}(t_{n+1}) =& S_{PREP0} + \psi(1-\tau)t_n^{\psi-1}G_2(t_n, S_{PREP}(t_n)) \\
&+ \frac{\tau\psi}{AB(\tau)\Gamma(\tau)}\int_0^{t_{n+1}}(t_{n+1}-s)^{\tau-1}S_{PREP}^{\psi-1}G_2(s, S_{PREP}(s))\,ds, \\
E_H(t_{n+1}) =& E_{H0} + \psi(1-\tau)t_n^{\psi-1}G_3(t_n, E_H(t_n)) \\
&+ \frac{\tau\psi}{AB(\tau)\Gamma(\tau)}\int_0^{t_{n+1}}(t_{n+1}-s)^{\tau-1}E_H^{\psi-1}G_3(s, E_H(s))\,ds, \\
E_{PEP}(t_{n+1}) =& E_{PEP0} + \psi(1-\tau)t_n^{\psi-1}G_4(t_n, E_{PEP}(t_n)) \\
&+ \frac{\tau\psi}{AB(\tau)\Gamma(\tau)}\int_0^{t_{n+1}}(t_{n+1}-s)^{\tau-1}E_{PEP}^{\psi-1}G_4(s, E_{PEP}(s))\,ds, \\
I_H(t_{n+1}) =& I_{H0} + \psi(1-\tau)t_n^{\psi-1}G_5(t_n, I_H(t_n)) \\
&+ \frac{\tau\psi}{AB(\tau)\Gamma(\tau)}\int_0^{t_{n+1}}(t_{n+1}-s)^{\tau-1}I_H^{\psi-1}G_5(s, I_H(s))\,ds, \\
A(t_{n+1}) =& A_0 + \psi(1-\tau)t_n^{\psi-1}G_6(t_n, A(t_n)) \\
&+ \frac{\tau\psi}{AB(\tau)\Gamma(\tau)}\int_0^{t_{n+1}}(t_{n+1}-s)^{\tau-1}A^{\psi-1}G_6(s, A(s))\,ds, \\
T_H(t_{n+1}) =& T_{H0} + \psi(1-\tau)t_n^{\psi-1}G_7(t_n, T_H(t_n)) \\
&+ \frac{\tau\psi}{AB(\tau)\Gamma(\tau)}\int_0^{t_{n+1}}(t_{n+1}-s)^{\tau-1}T_H^{\psi-1}G_7(s, T_H(s))\,ds, \qquad (38)
\end{aligned}
$$

So the numerical approximation of the integral is obtained as

$$
\begin{aligned}
S_H(t_{n+1}) =& S_{H0} + \frac{\psi(1-\tau)t_n^{\psi-1}G_1(t_n, S_H(t_n))}{AB(\tau)} \\
&+ \frac{\tau\psi}{AB(\tau)\Gamma(\tau)}\sum_{j=1}^{n}\int_{t_j}^{t_{j+1}}(t_{j+1}-s)^{\tau-1}S_H^{\psi-1}G_1(t_n, S_H^j(s))\,ds, \\
S_{PREP}(t_{n+1}) =& S_{PREP0} + \frac{\psi(1-\tau)t_n^{\psi-1}G_2(t_n, S_{PREP}(t_n))}{AB(\tau)} \\
&+ \frac{\tau\psi}{AB(\tau)\Gamma(\tau)}\sum_{j=1}^{n}\int_{t_j}^{t_{j+1}}(t_{j+1}-s)^{\tau-1}S_{PREP}^{\psi-1}G_2(t_n, S_{PREP}^j(s))\,ds, \\
E_H(t_{n+1}) =& E_{H0} + \frac{\psi(1-\tau)t_n^{\psi-1}G_3(t_n, E_H(t_n))}{AB(\tau)} \\
&+ \frac{\tau\psi}{AB(\tau)\Gamma(\tau)}\sum_{j=1}^{n}\int_{t_j}^{t_{j+1}}(t_{j+1}-s)^{\tau-1}E_H^{\psi-1}G_3(t_n, E_H^j(s))\,ds,
\end{aligned}
$$

$$
\begin{aligned}
E_{PEP}(t_{n+1}) =& E_{PEP0} + \frac{\psi(1-\tau)t_n^{\psi-1}G_4(t_n, E_{PEP}(t_n))}{AB(\tau)} \\
&+ \frac{\tau\psi}{AB(\tau)\Gamma(\tau)}\sum_{j=1}^{n}\int_{t_j}^{t_{j+1}}(t_{j+1}-s)^{\tau-1}E_{PEP}^{\psi-1}G_4(t_n, E_{PEP}^j(s))\,ds, \\
I_H(t_{n+1}) =& I_{H0} + \frac{\psi(1-\tau)t_n^{\psi-1}G_5(t_n, I_H(t_n))}{AB(\tau)} \\
&+ \frac{\tau\psi}{AB(\tau)\Gamma(\tau)}\sum_{j=1}^{n}\int_{t_j}^{t_{j+1}}(t_{j+1}-s)^{\tau-1}I_H^{\psi-1}G_5(t_n, I_H^j(s))\,ds, \\
A(t_{n+1}) =& A_0 + \frac{\psi(1-\tau)t_n^{\psi-1}G_6(t_n, A(t_n))}{AB(\tau)} \\
&+ \frac{\tau\psi}{AB(\tau)\Gamma(\tau)}\sum_{j=1}^{n}\int_{t_j}^{t_{j+1}}(t_{j+1}-s)^{\tau-1}A^{\psi-1}G_6(t_n, A^j(s))\,ds, \\
T_H(t_{n+1}) =& T_{H0} + \frac{\psi(1-\tau)t_n^{\psi-1}G_7(t_n, T_H(t_n))}{AB(\tau)} \\
&+ \frac{\tau\psi}{AB(\tau)\Gamma(\tau)}\sum_{j=1}^{n}\int_{t_j}^{t_{j+1}}(t_{j+1}-s)^{\tau-1}T_H^{\psi-1}G_7(t_n, T_H^j(s))\,ds,
\end{aligned}
\tag{39}
$$

Two-step Lagrange's interpolation polynomials with $\Delta t = t_{j+1} - t_j$ function as an estimate for the integrand functions on $[t_j, t_{j+1}]$. Thus, we obtain

$$
\begin{aligned}
S_H(t_{n+1}) =& S_{H0} + \frac{\psi(1-\tau)t_n^{\psi-1}G_1(t_n, S_H(t_n))}{AB(\tau)} \\
&+ \frac{\tau\psi}{AB(\tau)\Gamma(\tau)}\sum_{j=1}^{n}\int_{t_j}^{t_{j+1}}(t_{j+1}-s)^{\tau-1}S_H^{\psi-1}Z_j^{S_H}(s)\,ds, \\
S_{PREP}(t_{n+1}) =& S_{PREP0} + \frac{\psi(1-\tau)t_n^{\psi-1}G_2(t_n, S_{PREP}(t_n))}{AB(\tau)} \\
&+ \frac{\tau\psi}{AB(\tau)\Gamma(\tau)}\sum_{j=1}^{n}\int_{t_j}^{t_{j+1}}(t_{j+1}-s)^{\tau-1}S_{PREP}^{\psi-1}Z_j^{S_{PREP}}(s)\,ds, \\
E_H(t_{n+1}) =& E_{H0} + \frac{\psi(1-\tau)t_n^{\psi-1}G_3(t_n, E_H(t_n))}{AB(\tau)} \\
&+ \frac{\tau\psi}{AB(\tau)\Gamma(\tau)}\sum_{j=1}^{n}\int_{t_j}^{t_{j+1}}(t_{j+1}-s)^{\tau-1}E_H^{\psi-1}Z_j^{E_H}(s)\,ds, \\
E_{PEP}(t_{n+1}) =& E_{PEP0} + \frac{\psi(1-\tau)t_n^{\psi-1}G_4(t_n, E_{PEP}(t_n))}{AB(\tau)} \\
&+ \frac{\tau\psi}{AB(\tau)\Gamma(\tau)}\sum_{j=1}^{n}\int_{t_j}^{t_{j+1}}(t_{j+1}-s)^{\tau-1}E_{PEP}^{\psi-1}Z_j^{E_{PEP}}(s)\,ds,
\end{aligned}
$$

$$
\begin{aligned}
I_H(t_{n+1}) =& I_{H0} + \frac{\psi(1-\tau)t_n^{\psi-1}G_5(t_n, I_H(t_n))}{AB(\tau)} \\
&+ \frac{\tau\psi}{AB(\tau)\Gamma(\tau)}\sum_{j=1}^{n}\int_{t_j}^{t_{j+1}}(t_{j+1}-s)^{\tau-1}I_H^{\psi-1}Z_j^{I_H}(s)\,ds, \\
A(t_{n+1}) =& A_0 + \frac{\psi(1-\tau)t_n^{\psi-1}G_6(t_n, A(t_n))}{AB(\tau)} \\
&+ \frac{\tau\psi}{AB(\tau)\Gamma(\tau)}\sum_{j=1}^{n}\int_{t_j}^{t_{j+1}}(t_{j+1}-s)^{\tau-1}A^{\psi-1}Z_j^{A}(s)\,ds, \\
T_H(t_{n+1}) =& T_{H0} + \frac{\psi(1-\tau)t_n^{\psi-1}G_7(t_n, T_H(t_n))}{AB(\tau)} \\
&+ \frac{\tau\psi}{AB(\tau)\Gamma(\tau)}\sum_{j=1}^{n}\int_{t_j}^{t_{j+1}}(t_{j+1}-s)^{\tau-1}T_H^{\psi-1}Z_j^{T_H}(s)\,ds,
\end{aligned} \tag{40}
$$

where

$$
\begin{aligned}
Z_j^{S_H}(s) =& \frac{s-t_{j-1}}{t_j-t_{j-1}}t_j^{\psi-1}G_1(s, S_H^j(s)) - \frac{s-t_{j-1}}{t_j-t_{j-1}}t_{j-1}^{\psi-1}G_1(s, S_H^{j-1}(s)), \\
Z_j^{S_{PREP}}(s) =& \frac{s-t_{j-1}}{t_j-t_{j-1}}t_j^{\psi-1}G_2(s, S_{PREP}^j(s)) \\
&- \frac{s-t_{j-1}}{t_j-t_{j-1}}t_{j-1}^{\psi-1}G_2(s, S_{PREP}^{j-1}(s)), \\
Z_j^{E_H}(s) =& \frac{s-t_{j-1}}{t_j-t_{j-1}}t_j^{\psi-1}G_3(s, E_H^j(s)) - \frac{s-t_{j-1}}{t_j-t_{j-1}}t_{j-1}^{\psi-1}G_3(s, E_H^{j-1}(s)), \\
Z_j^{E_{PEP}}(s) =& \frac{s-t_{j-1}}{t_j-t_{j-1}}t_j^{\psi-1}G_4(s, E_{PEP}^j(s)) - \frac{s-t_{j-1}}{t_j-t_{j-1}}t_{j-1}^{\psi-1}G_4(s, E_{PEP}^{j-1}(s)), \\
Z_j^{I_H}(s) =& \frac{s-t_{j-1}}{t_j-t_{j-1}}t_j^{\psi-1}G_5(s, I_H^j(s)) - \frac{s-t_{j-1}}{t_j-t_{j-1}}t_{j-1}^{\psi-1}G_5(s, I_H^{j-1}(s)), \\
Z_j^{A}(s) =& \frac{s-t_{j-1}}{t_j-t_{j-1}}t_j^{\psi-1}G_6(s, A^j(s)) - \frac{s-t_{j-1}}{t_j-t_{j-1}}t_{j-1}^{\psi-1}G_6(s, A^{j-1}(s)), \\
Z_j^{T_H}(s) =& \frac{s-t_{j-1}}{t_j-t_{j-1}}t_j^{\psi-1}G_7(s, T_H^j(s)) - \frac{s-t_{j-1}}{t_j-t_{j-1}}t_{j-1}^{\psi-1}G_7(s, T_H^{j-1}(s)).
\end{aligned} \tag{41}
$$

We finally solve the schemes needed for numerical calculations of the HIV/AIDS model (1):

$$
\begin{aligned}
S_H(t_{n+1}) =& S_{H0} + \psi(1-\tau)t_n^{\psi-1}G_1(t_n, S_H(t_n)) \\
&+ \frac{\psi(\Delta t)^{\tau}}{AB(\tau)\Gamma(\tau+2)}\sum_{j=1}^{n}\Big[t_j^{\psi-1}G_1(s, S_H^j(s))X_1(n,j) \\
&- t_{j-1}^{\psi-1}G_1(s, S_H^{j-1}(s))X_2(n,j)\Big], \\
S_{PREP}(t_{n+1}) =& S_{PREP0} + \psi(1-\tau)t_n^{\psi-1}G_2(t_n, S_{PREP}(t_n))
\end{aligned} \tag{42}
$$

$$+\frac{\psi(\Delta t)^{\tau}}{AB(\tau)\Gamma(\tau+2)}\sum_{j=1}^{n}\Big[t_j^{\psi-1}G_2(s,S_{PREP}^{j}(s))X_1(n,j) \tag{43}$$
$$-t_{j-1}^{\psi-1}G_2(s,S_{PREP}^{j-1}(s))X_2(n,j)\Big],$$
$$E_H(t_{n+1}) = E_{H0}+\psi(1-\tau)t_n^{\psi-1}G_3(t_n,E_H(t_n))$$
$$+\frac{\psi(\Delta t)^{\tau}}{AB(\tau)\Gamma(\tau+2)}\sum_{j=1}^{n}\Big[t_j^{\psi-1}G_3(s,E_H^{j}(s))X_1(n,j) \tag{44}$$
$$-t_{j-1}^{\psi-1}G_3(s,E_H^{j-1}(s))X_2(n,j)\Big],$$
$$E_{PEP}(t_{n+1}) = E_{PEP0}+\psi(1-\tau)t_n^{\psi-1}G_4(t_n,E_{PEP}(t_n))$$
$$+\frac{\psi(\Delta t)^{\tau}}{AB(\tau)\Gamma(\tau+2)}\sum_{j=1}^{n}\Big[t_j^{\psi-1}G_4(s,E_{PEP}^{j}(s))X_1(n,j)- \tag{45}$$
$$t_{j-1}^{\psi-1}G_4(s,E_{PEP}^{j-1}(s))X_2(n,j)\Big],$$
$$I_H(t_{n+1}) = I_{H0}+\psi(1-\tau)t_n^{\psi-1}G_5(t_n,I_H(t_n))$$
$$+\frac{\psi(\Delta t)^{\tau}}{AB(\tau)\Gamma(\tau+2)}\sum_{j=1}^{n}\Big[t_j^{\psi-1}G_5(s,I_H^{j}(s))X_1(n,j) \tag{46}$$
$$-t_{j-1}^{\psi-1}G_5(s,I_H^{j-1}(s))X_2(n,j)\Big],$$
$$A(t_{n+1}) = A_0+\psi(1-\tau)t_n^{\psi-1}G_6(t_n,A(t_n))$$
$$+\frac{\psi(\Delta t)^{\tau}}{AB(\tau)\Gamma(\tau+2)}\sum_{j=1}^{n}\Big[t_j^{\psi-1}G_6(s,A^{j}(s))X_1(n,j) \tag{47}$$
$$-t_{j-1}^{\psi-1}G_6(s,A^{j-1}(s))X_2(n,j)\Big],$$
$$T_H(t_{n+1}) = T_{H0}+\psi(1-\tau)t_n^{\psi-1}G_7(t_n,T_H(t_n))$$
$$+\frac{\psi(\Delta t)^{\tau}}{AB(\tau)\Gamma(\tau+2)}\sum_{j=1}^{n}\Big[t_j^{\psi-1}G_7(s,T_H^{j}(s))X_1(n,j) \tag{48}$$
$$-t_{j-1}^{\psi-1}G_7(s,T_H^{j-1}(s))X_2(n,j)\Big], \tag{49}$$

where

$$\begin{aligned} X_1(n,j) &= (n+1-j)^{\tau+1}-(n-j)^{\tau}-(n-j)^{\tau}(n-j+2+2\tau),\\ X_2(n,j) &= (n+1-j)^{\tau+1}-(n-j)^{\tau}-(n-j)^{\tau}(n-j+1+\tau). \end{aligned} \tag{50}$$

The biological implication of this fractal-fractional numerical scheme is that it enables accurate, long-term simulation of HIV dynamics in populations where past exposure, treatment history, and behavioral memory significantly influence future infection risk—effects that standard models often ignore. By incorporating both fractional-order memory (capturing long-term immune or behavioral effects) and fractal dimensions (modeling heterogeneous contact patterns),

this method produces realistic epidemic curves that align with observed data in high-burden settings. For public health, this means trustworthy projections of new infections, treatment demand, and intervention impact over decades. Policymakers can now simulate "what-if" scenarios—such as scaling PrEP to 70% coverage or achieving 95% viral suppression—and obtain credible forecasts of whether elimination is feasible by 2030. This tool transforms abstract theory into actionable intelligence, guiding resource allocation, program design, and global HIV strategy with unprecedented precision.

4.4 Uncertainty and sensitivity analysis of the HIV/AIDS model

Variations are predicted because the model includes several parameters, and calculating their values for numerical simulations involves inherent errors. We used Latin Hypercube Sampling (LHS) to sample values for the parameters that affect the infected populations and the reproduction number, following the methodology in [16]. To evaluate the connection between parameter values and the sensitivity analysis final results, we calculated the Partial Rank Correlation Coefficient (PRCC). For every iteration of LHS, 1,000 simulations were run. The PRCC analysis determined the most critical parameters by using the basic reproduction number (R_{0H}) as the response function. These were the natural death rate (θ_H), the progression rate from HIV infection to the AIDS stage (ρ_1), the contact rate (γ_H), and the rate at which AIDS patients transition to treatment (θ_2).

As seen in Tables 2–3 and Figures 2–3, the sensitivity analysis reveals that the natural death rate (θ_H) has the strongest negative correlation (PRCC = -0.167, $p < 0.05$) with the reproduction number, indicating that higher natural mortality rates significantly decrease disease transmission potential. This parameter is the only one statistically significant at the $p < 0.05$ level. The progression rate from HIV infected individuals to the AIDS class (ρ_1) shows a positive correlation (PRCC = +0.136, $p = 0.054$), suggesting that a higher progression rate from the HIV-infected class to the AIDS infected class increases transmission potential, although this effect is marginally significant. Similarly, the contact rate (γ_H) demonstrates a positive correlation (PRCC = +0.133, $p = 0.061$), indicating that increased contact rates contribute to higher transmission. The progression rate from AIDS to treatment (θ_2) shows a negative correlation (PRCC = -0.128, $p = 0.072$), suggesting that faster initiation of treatment for AIDS patients may help reduce transmission. The disease-induced death rate for infected individuals (δ_I) shows a negative correlation (PRCC = -0.101, $p = 0.156$), while the proportion of exposed individuals

taking PEP (θ) also demonstrates a negative correlation (PRCC = -0.095, $p = 0.181$), suggesting that increased PEP uptake will contribute to reduced transmission. The parameter (γ) which accounts for the number of sexual parameters by an individual shows a positive correlation (PRCC = +0.089, $p = 0.211$) which suggest that an increase in the number of sexual partners by an individual will significantly increase the probability of contraction of HIV/AIDS as well as increasing the spread of the disease in the human population, while the compliance rate for condom usage (ς) shows a negative correlation (PRCC = -0.087, $p = 0.221$) suggesting that an increase in the rate of compliance to this parameter will substantially reduce the transmission of HIV/AIDS in the human population. The progression rate of HIV-infected individuals into antiretroviral treatment (θ_1) demonstrates a negative correlation (PRCC = -0.083, $p = 0.243$), and condom efficacy (Ψ) shows a negative correlation (PRCC = -0.082, $p = 0.251$), suggesting that harnessing these measures will reduce the burden of the disease in the population.

Parameters with lower PRCC values include the efficacy of PEP (ϵ_2), modification parameters for transmission in the treatment class (η), the rate at which treated individuals return to the HIV-infected class (χ), the failure rate of PEP (σ_2), proportion of individuals utilizing PrEP (Θ), efficacy of PrEP (ϵ_1), waning rate of protection (ω_H), disease-induced death rate for treated individuals (δ_T), recruitment rate into the susceptible class (Λ), progression rate of exposed individuals (σ_1), and disease-induced death rate for AIDS cases (δ_A). Based on these sensitivity analysis results, public health interventions should focus on strategies that influence mortality and demographic factors (θ_H), control progression rate from HIV infected individuals to the AIDS class (ρ_1), reduce contact rates (γ_H), and accelerate the initiation of treatment among AIDS patients (θ_2). While not statistically significant at conventional levels, interventions targeting the disease-induced death rate (δ_I) and PEP uptake (θ) may also contribute to controlling HIV/AIDS transmission in the population.

4.5 HIV/AIDS data fitting and forecasting analysis for South Africa

The HIV/AIDS data fitting and forecasting analysis for South Africa draws on historical statistics from 2010 to 2023 as presented in Table 4, sourced from UNAIDS global AIDS reports [46]. The dataset includes three key indicators: People living with HIV (PLHIV), new HIV infections, and ART coverage, measured as the percentage of PLHIV receiving treatment. These indicators

Table 2: PRCC Values (sorted by influence)

Rank	Parameter	PRCC	p-value
1	θ_H	-0.167302	0.017890
2	ρ_1	+0.136342	0.054219
3	γ_H	+0.132929	0.060593
4	θ_2	-0.127707	0.071528
5	δ_I	-0.100702	0.155952
6	θ	-0.095054	0.180612
7	γ	+0.088736	0.211477
8	ς	-0.086949	0.220853
9	θ_1	-0.082919	0.243083
10	Ψ	-0.081597	0.250704
11	ϵ_2	-0.079809	0.261274
12	η	-0.070033	0.324419
13	χ	-0.059325	0.404026
14	σ_2	+0.049524	0.486172
15	Θ	-0.048354	0.496546
16	ϵ_1	-0.032523	0.647536
17	ω_H	-0.025780	0.717089
18	δ_T	-0.024852	0.726851
19	Λ	+0.020503	0.773220
20	σ_1	+0.017072	0.810373
21	δ_A	-0.007588	0.915075

Table 3: PRCC Values for Top 10 Parameters.

Rank	Parameter	PRCC	p-value
1	θ_H	+0.167302	0.017890
2	ρ_1	+0.136342	0.054219
3	γ_H	+0.132929	0.060593
4	θ_2	-0.127707	0.071528
5	δ_I	-0.100702	0.155952
6	θ	-0.095054	0.180612
7	γ	+0.088736	0.211477
8	ς	-0.086949	0.220853
9	θ_1	-0.082919	0.243083
10	Ψ	-0.081597	0.250704

formed the empirical basis for a mathematical modeling approach aimed at estimating parameters and forecasting the future trajectory of the HIV epidemic in the country. The model applied is a compartmental structure capturing the dynamics of HIV transmission and treatment. It incorporates natural population growth and mortality (represented by birth and death rates, Λ and θ_H), transmission dynamics (via transmission coefficient γ_H), progression from HIV to AIDS, ART uptake and treatment efficacy, and different mortality outcomes depending on treatment

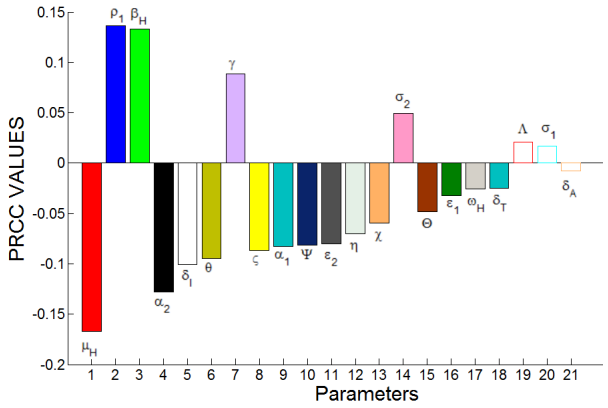

Figure 2: An extended PRCC analysis showing the correlation of all 21 model parameters with the HIV/AIDS basic reproduction number (R_{0H}). The visualization reveals the complex interplay of various factors affecting HIV transmission, including mortality rates, progression rates, and preventive interventions.

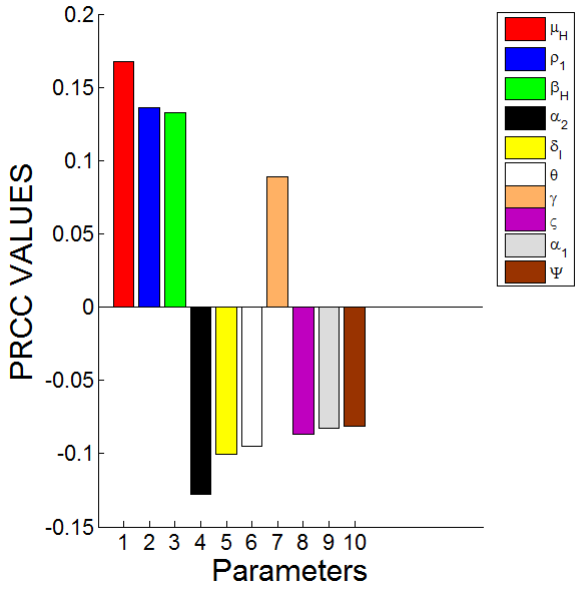

Figure 3: A bar graph displaying the sensitivity of the basic reproduction number (R_{0H}) to the top 10 model parameters. The graph highlights the most influential parameters, with notable positive and negative correlations, demonstrating the relative impact of different epidemiological factors on HIV transmission dynamics.

status. Parameter estimation was performed using MATLAB's `fmincon` optimization routine, which allows for constrained nonlinear optimization - ensuring that the model fit respects biological plausibility while accurately reproducing observed data trends.

The optimization process yielded 21 estimated parameters, with notable outcomes including a transmission coefficient of $\gamma_H = 0.0655$, along with multiple parameters describing treatment initiation and mortality differentials. The model aligns closely with observed data, as demonstrated in the graphical output (4a), where the model's red line accurately traces the trend in new HIV infections from 2018 to 2023. With this validated model, a forecast was generated covering the period from 2024 to 2033. The projections indicate a steady decline in new HIV infections, decreasing from approximately 200,213 in 2024 to 143,880 in 2033, marking a 28% reduction. Simultaneously, the number of individuals receiving ART is projected to grow, albeit at a slower rate, from 4.7 million in 2024 to 4.35 million in 2033. The number of untreated individuals with HIV or AIDS is expected to decline from 115,787 in 2024 to 101,785 in 2030, after which it stabilizes near 100,000. These trends suggest a substantial shift in the epidemic profile, with a growing dominance of the treated population, as illustrated by the yellow area in Figure 4b. Epidemiologically, the analysis underscores the success of South Africa's ART expansion, which has converted HIV into a manageable chronic condition for a majority of those infected. The epidemic has entered a mature control phase marked by high treatment coverage and falling incidence. Nevertheless, the persistence of approximately 100,000 untreated individuals highlights ongoing challenges in diagnosis, linkage to care, and adherence. From a public health perspective, the forecast aligns with global epidemic control targets but also points to the need for renewed efforts to reach marginalized populations.

Table 4: HIV Statistics for South Africa (2010-2023) [46].

Year	**People living with HIV**	**New HIV infections**	**ART coverage (%)**
2010	6,100,000	380,000	16
2011	6,300,000	370,000	19
2012	6,500,000	360,000	22
2013	6,700,000	350,000	29
2014	6,800,000	340,000	35
2015	7,000,000	330,000	45
2016	7,100,000	310,000	53
2017	7,200,000	300,000	61
2018	7,400,000	280,000	68
2019	7,500,000	240,000	71
2020	7,600,000	230,000	72
2021	7,700,000	210,000	75
2022	7,800,000	200,000	77
2023	7,900,000	190,000	79

Table 5: South Africa HIV/AIDS Indicators and Projection: New Infections, Untreated, and Treated PLHIV (2010–2033).

Year	New Infections	Untreated	Treated
2022	218272	128353	4843674
2023	208933	124745	4789972
2024	200213	115787	4744012
2025	191680	107609	4698742
2026	184949	105355	4658007
2027	177023	104067	4606564
2028	170070	103155	4558881
2029	165040	102502	4522845
2030	159648	101785	4482653
2031	153981	101003	4438531
2032	148124	100156	4390692
2033	143880	99518	4354472

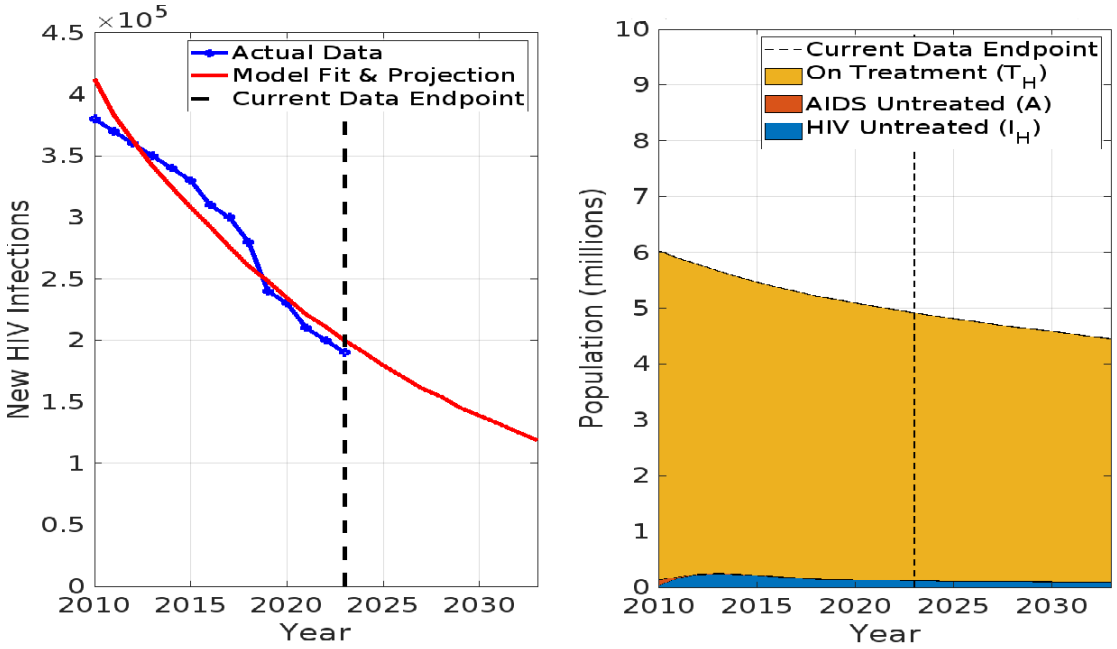

(a) (b)

Figure 4: A time series plot (4a) comparing actual and projected new HIV infections in South Africa from 2010 to 2030. The graph illustrates the historical trend and the model's predictive projection, showing a consistent decline in new infections over time, and (4b) shows a stacked area chart depicting the changing population of HIV/AIDS patients in different states (on treatment, untreated HIV, and untreated AIDS) from 2010 to 2030. The visualization highlights shifting demographics of HIV/AIDS management in South Africa.

Table 6: Fitted parameter values for the HIV/AIDS model.

Parameter	Value	Range (per year)	Reference
Λ	0.0070	[0.0056, 0.0084]	Fitted
γ_H	0.0655	[0.0524, 0.0786]	Fitted
γ	1.4069	[1.1255, 1.6883]	Fitted
ς	0.9961	[0.7969, 1.1953]	Fitted
Ψ	0.1514	[0.1211, 0.1817]	Fitted
θ_H	0.0016	[0.0013, 0.0019]	Fitted
η	0.9959	[0.7967, 1.1951]	Fitted
ω_H	0.0413	[0.0330, 0.0496]	Fitted
ε_1	0.8463	[0.6770, 1.0156]	Fitted
σ_1	0.0119	[0.0095, 0.0143]	Fitted
θ	0.9573	[0.7658, 1.1488]	Fitted
σ_2	0.0834	[0.0667, 0.1001]	Fitted
ε_2	0.9370	[0.7496, 1.1244]	Fitted
θ_1	1.3025	[1.0420, 1.5630]	Fitted
ρ_1	0.0968	[0.0774, 0.1162]	Fitted
θ_2	0.1867	[0.1494, 0.2240]	Fitted
δ_I	0.3357	[0.2686, 0.4028]	Fitted
δ_A	1.9944	[1.5955, 2.3933]	Fitted
δ_T	0.0324	[0.0259, 0.0389]	Fitted
δ_V	0.0008	[0.0006, 0.0010]	Fitted
χ	0.0349	[0.0279, 0.0419]	Fitted
Θ	0.0022	[0.0018, 0.0026]	Fitted

4.6 Numerical simulations of HIV/AIDS model

Utilizing the parameter values obtained from fitting the HIV/AIDS model (1) to the South African HIV/AIDS data (Tables 4–5), as outlined in Table 6, we present the graphs of the numerical simulations of the model.

Figure 5a presents a two-dimensional plot with time (in days) on the x-axis and the number of susceptible individuals (S_H) on the y-axis, ranging from approximately 1.93 to 2.00 (in units of 10^6). The graph features multiple overlapping curves, each representing a different fractional order τ (from 0.55 to 0.95), with colors ranging from purple ($\tau = 0.55$) to yellow ($\tau = 0.95$). Initially, all curves start at a high value and exhibit a sharp decline, followed by oscillatory behavior that stabilizes over time, with lower τ values showing a slower decline and higher steady-state values compared to higher τ values. Figure 5a reflects the dynamics of the susceptible population under varying fractional orders τ, which model memory effects and nonlocal interactions in HIV transmission. A lower τ indicates a slower depletion of susceptible individuals due to prolonged memory effects, suggesting that interventions like awareness or behavioral changes have a delayed but sustained impact. As τ approaches 1, the rapid decline aligns with classi-

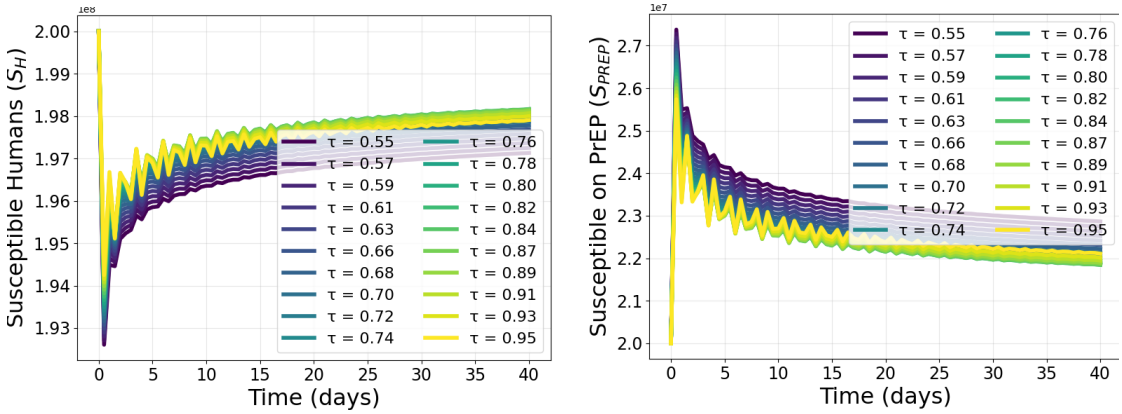

(a) (b)

Figure 5: Impact of fractional order τ on susceptible populations.

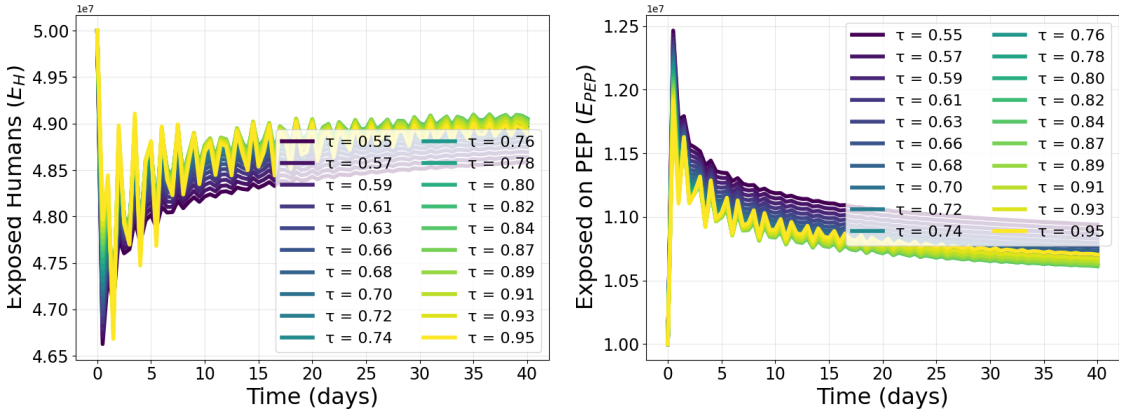

(a) (b)

Figure 6: Fractional order effects on exposed populations.

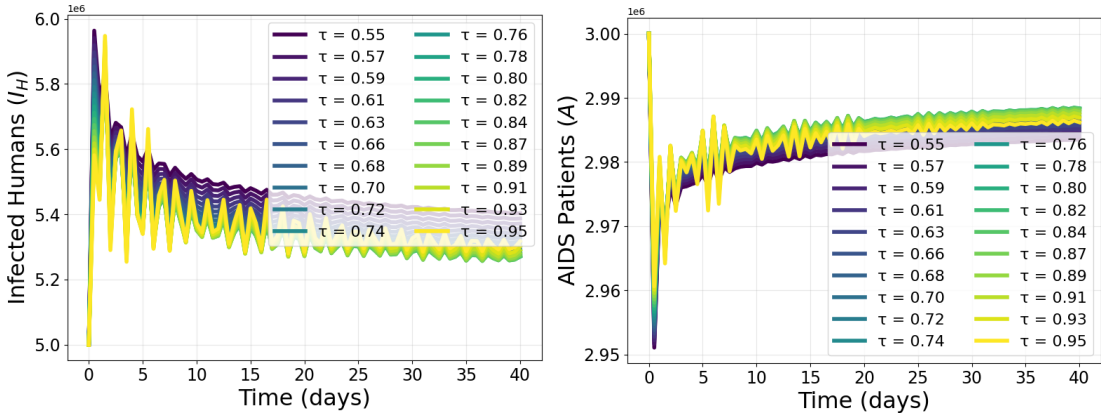

(a) (b)

Figure 7: Disease progression dynamics under fractional order variations.

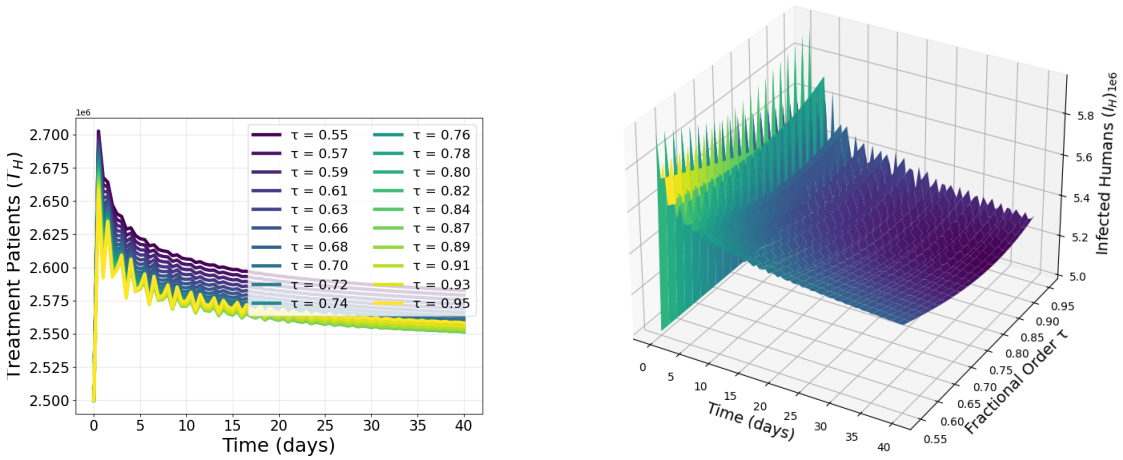

(a) (b)

Figure 8: Treatment dynamics and three-dimensional infection analysis.

cal integer-order models, indicating a faster transition to exposure due to immediate infectious contacts. Figure 5b displays a two-dimensional plot with time (in days) on the x-axis and the number of susceptible individuals on PrEP (S_{PrEP}) on the y-axis, ranging from approximately 2.0 to 2.7 (in units of 10^7). Similar to Figure 5a, it features multiple curves for different τ values (0.55 to 0.95), with colors transitioning from purple to yellow. The curves show an initial peak followed by a gradual decline with oscillations, where lower τ values result in higher and more sustained S_{PrEP} levels over time. Figure 5b illustrates the impact of PrEP effectiveness across different fractional orders. Lower τ values suggest a prolonged protective effect of PrEP, reflect-

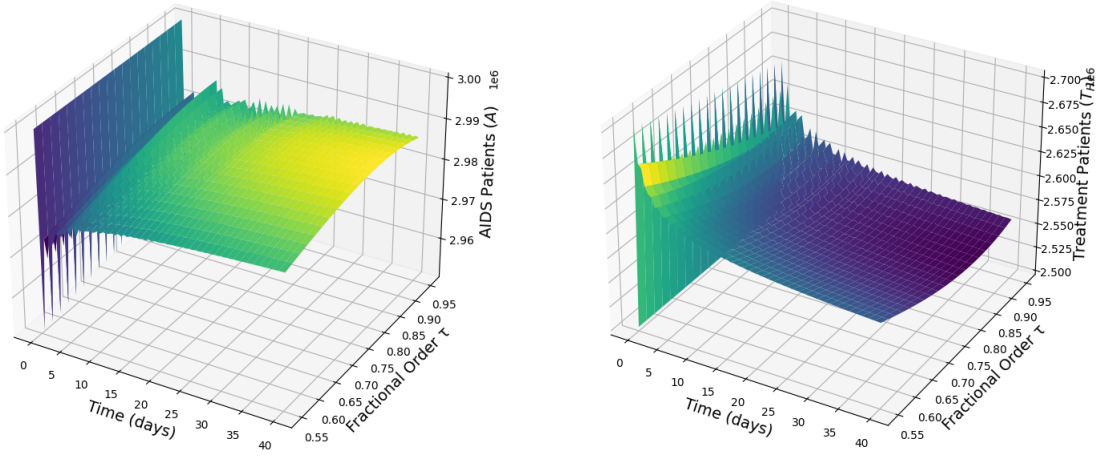

(a) (b)

Figure 9: Three-dimensional surface plots of advanced disease stages and treatment.

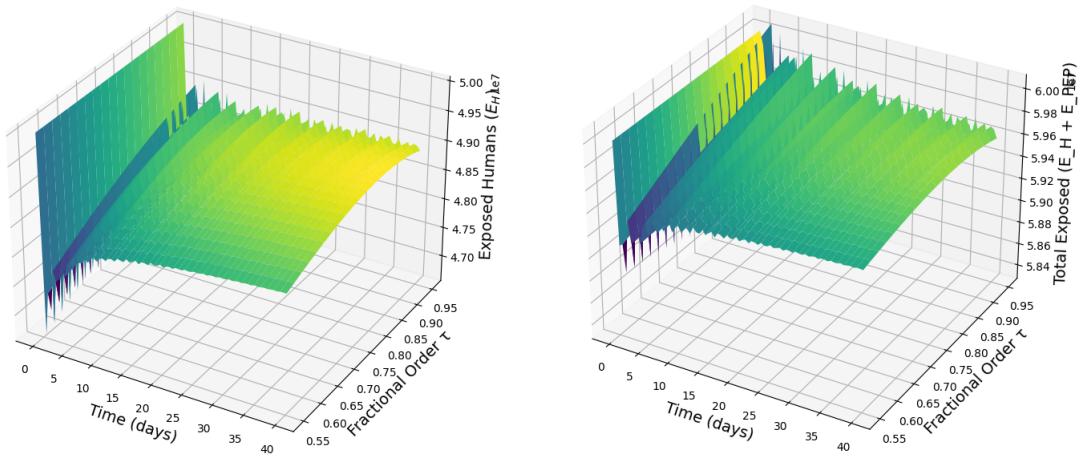

(a) (b)

Figure 10: Combined exposure dynamics in three-dimensional analysis.

ing slower transitions to exposure due to memory in prophylactic adherence. This indicates that populations with stronger historical adherence to PrEP maintain higher susceptible numbers longer, highlighting the importance of consistent PrEP use in reducing HIV incidence. Figure 6a presents a two-dimensional plot with time (in days) on the x-axis and the number of exposed individuals (E_H) on the y-axis, ranging from approximately 4.65 to 5.00 (in units of 10^7). It includes multiple curves for τ values from 0.55 to 0.95, with colors from purple to yellow. The curves start high, decline sharply, and then stabilize with oscillations, where lower τ values lead

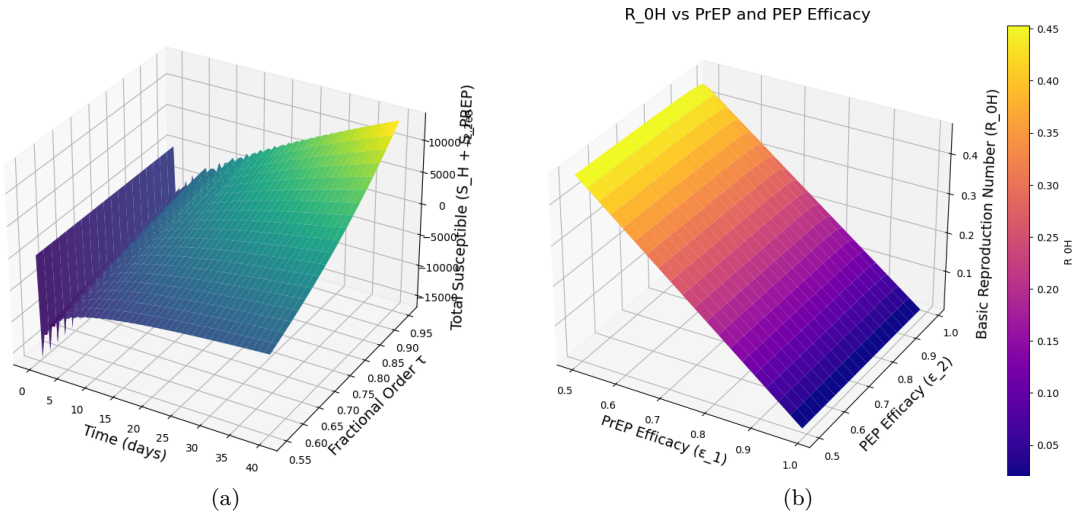

(a) (b)

Figure 11: Susceptible population dynamics and prophylaxis efficacy analysis.

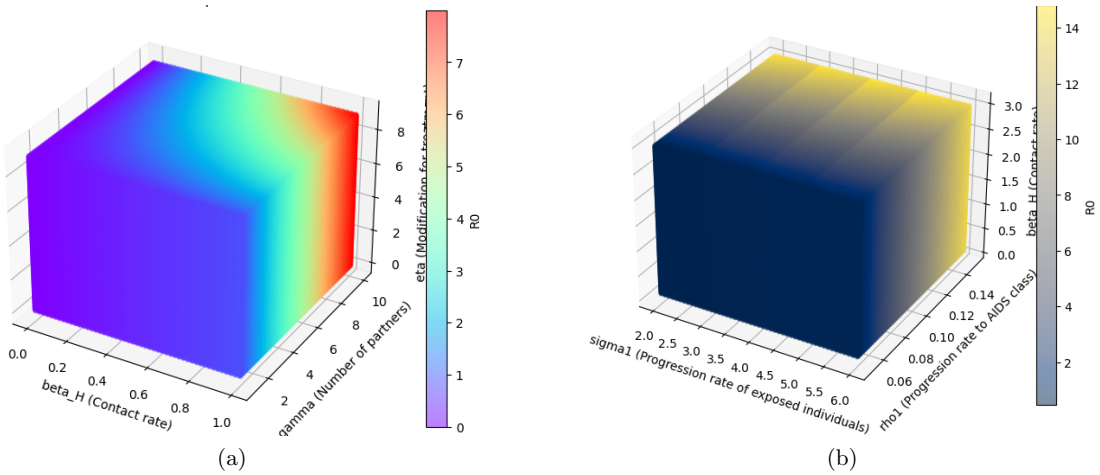

(a) (b)

Figure 12: Parameter sensitivity analysis for transmission dynamics.

to higher steady-state exposed populations compared to higher τ values. Figure 6a shows how the exposed population evolves with fractional order τ, capturing the latency period before infection. Lower τ values indicate a slower progression from exposure to infection, possibly due to memory effects in immune response or delayed contact tracing. This suggests that interventions targeting early exposure stages may be more effective in populations with lower τ, where the exposed pool persists longer.

Figure 6b displays a two-dimensional plot with time (in days) on the x-axis and the number

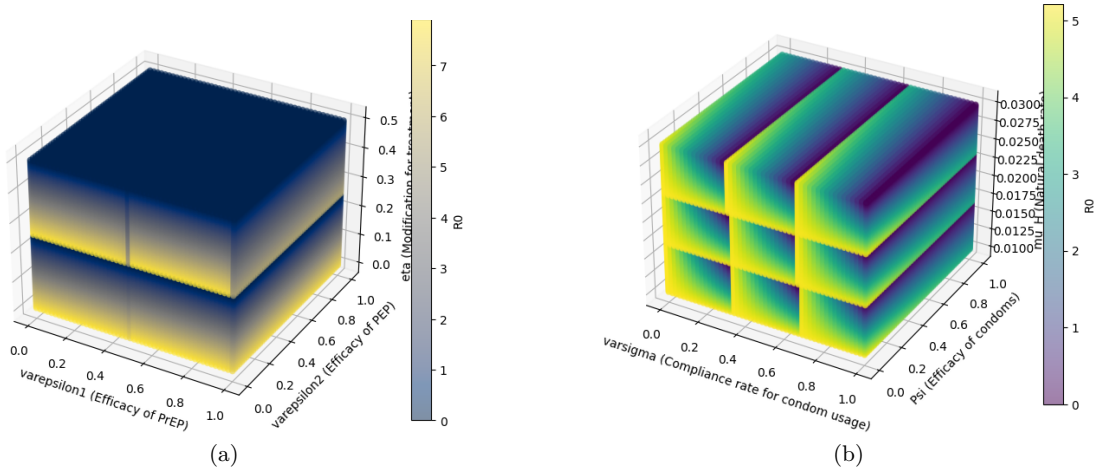

(a) (b)

Figure 13: Intervention efficacy and behavioral parameter analysis.

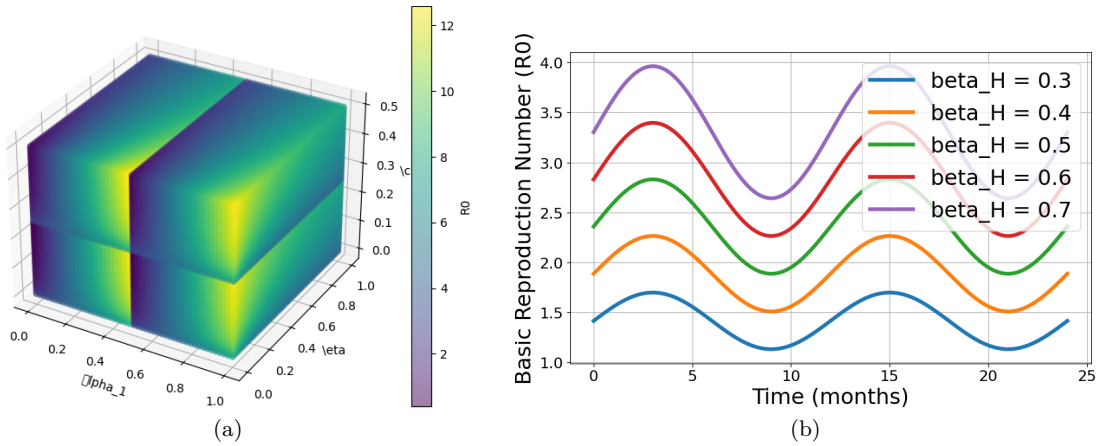

(a) (b)

Figure 14: Treatment dynamics and temporal reproduction number analysis.

of exposed individuals on PEP (E_{PEP}) on the y-axis, ranging from approximately 1.00 to 1.25 (in units of 10^7). It features curves for τ values from 0.55 to 0.95, with colors from purple to yellow. The curves show an initial peak followed by a steady decline with minor oscillations, with lower τ values maintaining higher E_{PEP} levels over time. Figure 6b represents the dynamics of individuals using PEP during the exposed phase. Lower τ values suggest a prolonged presence of exposed individuals on PEP, reflecting memory effects in treatment adherence or efficacy. This indicates that PEP's protective role is more sustained in populations with lower τ, emphasizing the need for timely and consistent PEP administration to prevent progression to infection. Figure 7a presents a two-dimensional plot with time (in days) on the x-axis and the number of

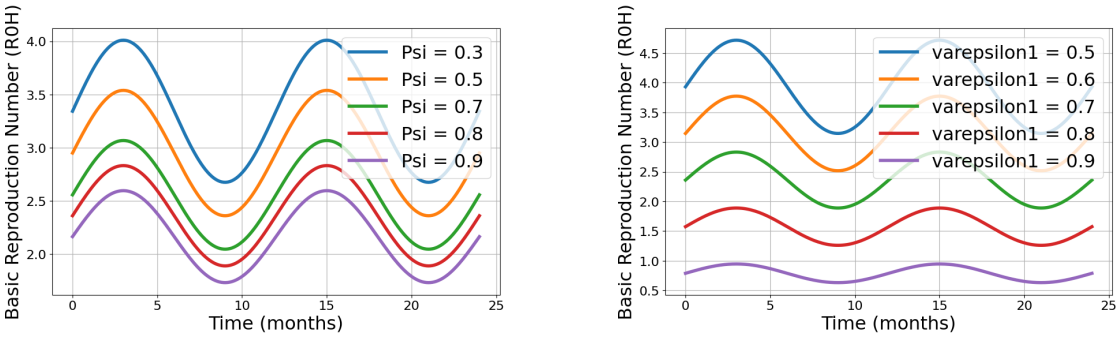

Figure 15: Temporal analysis of prevention intervention efficacy.

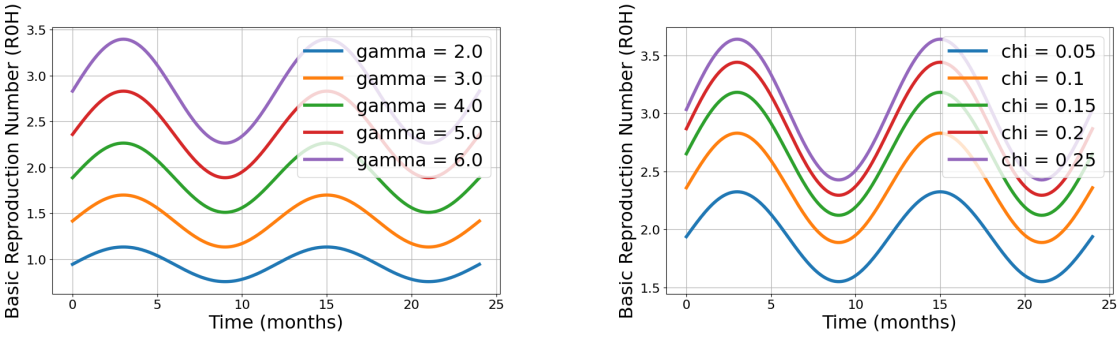

Figure 16: Sexual behavior and treatment reversion effects on transmission dynamics.

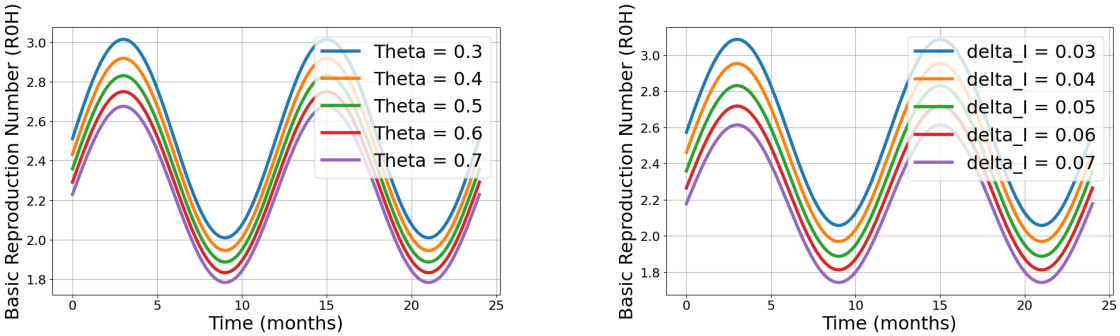

Figure 17: Mortality effects on reproduction number dynamics.

infected individuals (I_H) on the y-axis, ranging from approximately 5.0 to 6.0 (in units of 10^6). It

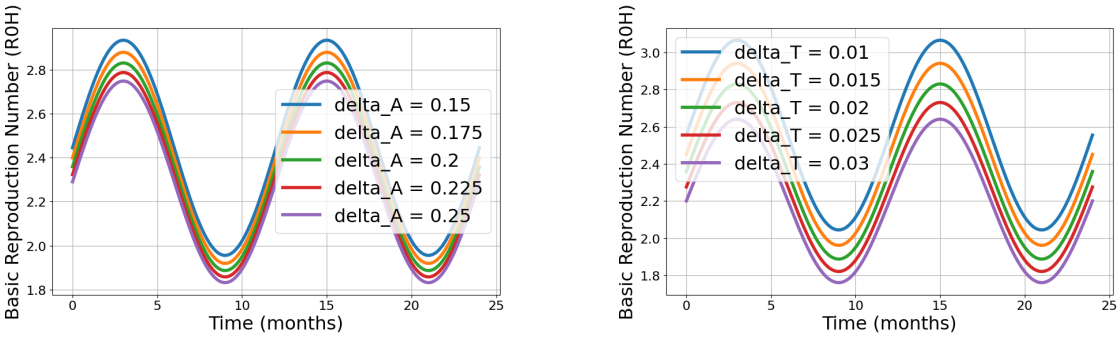

Figure 18: Stage-specific mortality impacts on transmission control.

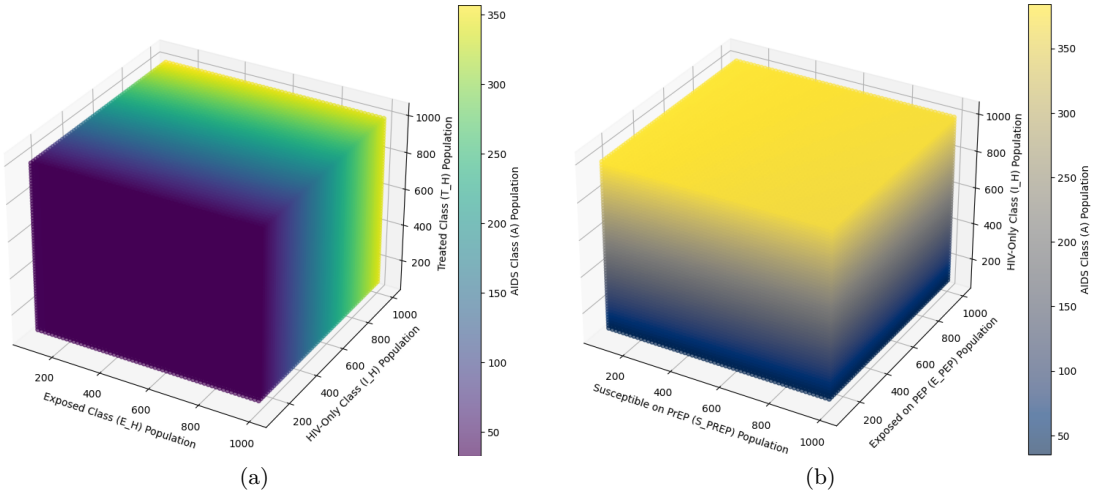

Figure 19: Multi-compartment interaction analysis and prophylaxis strategy evaluation.

includes curves for τ values from 0.55 to 0.95, with colors from purple to yellow. The curves show an initial peak followed by a decline with oscillatory stabilization, where lower τ values result in higher and more persistent infected populations. Figure 7a depicts the progression of HIV-only infected individuals, with lower τ values indicating slower disease progression due to memory effects in immune response or treatment uptake. This suggests that populations with lower τ may experience prolonged infectious periods, necessitating targeted interventions like ART to reduce transmission rates. Figure 7b displays a two-dimensional plot with time (in days) on the x-axis and the number of individuals with HIV/AIDS (A) on the y-axis, ranging from approximately 2.95 to 3.00 (in units of 10^6). It features curves for τ values from 0.55 to 0.95, with colors from purple to yellow. The curves show an initial increase followed by stabilization with oscillations,

where lower τ values lead to slightly higher AIDS cases over time. Figure 7b illustrates the progression to advanced HIV/AIDS, with lower τ values suggesting a slower transition from HIV to AIDS due to memory effects in disease progression or treatment delays. This indicates that populations with lower τ may have a prolonged pre-AIDS phase, highlighting the need for early ART to prevent progression to AIDS. Figure 8a presents a two-dimensional plot with time (in days) on the x-axis and the number of individuals on ART (T_H) on the y-axis, ranging from approximately 2.50 to 2.70 (in units of 10^6). It includes curves for τ values from 0.55 to 0.95, with colors from purple to yellow. The curves show an initial decline followed by stabilization with oscillations, where lower τ values maintain higher treatment numbers over time. Figure 8a reflects the dynamics of individuals on ART, with lower τ values indicating a sustained treatment population due to memory effects in therapy adherence or access. This suggests that consistent ART programs are crucial in populations with lower τ, where treatment effects persist longer, reducing mortality and transmission. Figure 8b displays a three-dimensional surface plot with time (in days) on the x-axis, fractional order τ on the y-axis (0.55 to 0.95), and the number of infected individuals (I_H) on the z-axis (5.0 to 5.8 in units of 10^6). The surface shows a peak at early times and lower τ, gradually flattening as time and τ increase, with a color gradient from purple to yellow indicating the density of infected cases. Biologically, Figure 8b provides a comprehensive view of how infection rates vary with time and fractional order, with lower τ values and early times showing higher infection peaks. This suggests that memory effects amplify initial infection spreads, underscoring the importance of early interventions to curb the epidemic in such scenarios.

Figure 9a presents a three-dimensional surface plot with time (in days) on the x-axis, fractional order τ on the y-axis (0.55 to 0.95), and the number of AIDS cases (A) on the z-axis (2.96 to 3.00 in units of 10^6). The surface shows a gradual rise and stabilization, with a color gradient from purple to yellow, where lower τ values maintain slightly higher AIDS levels over time. Figure 9a illustrates the temporal and fractional order dependence of AIDS progression, with lower τ values indicating a prolonged disease course. This highlights the need for sustained ART and support to manage advanced cases, especially in populations with significant memory effects. Figure 9b displays a three-dimensional surface plot with time (in days) on the x-axis, fractional order τ on the y-axis (0.55 to 0.95), and the number of individuals on treatment (T_H) on the z-axis (2.50 to 2.70 in units of 10^6). The surface shows an initial decline followed by stabilization, with a color gradient from purple to yellow, where lower τ values sustain higher treatment levels. Figure 9b reflects the interplay of time and fractional order on treatment dynamics, with lower τ values suggesting prolonged treatment efficacy due to memory effects. This indicates that consistent ART access is vital in populations with lower τ, where treatment benefits persist longer, improving survival rates.

Figure 10a is a three-dimensional surface plot with axes labeled as Time (days) ranging from 0 to 40, Fractional Order τ from 0.55 to 0.95, and Total Exposed Humans ($E_H + E_{PEP}$) scaled from approximately 4.70×10^7 to 5.00×10^7. The surface exhibits a color gradient from purple (lower values) to yellow (higher values), showing a jagged, oscillatory elevation that increases sharply with time, particularly at lower τ, with pronounced peaks and valleys along the time axis, forming a ridged terrain that smooths slightly at higher τ. Figure 10a demonstrates the impact of fractional order τ on the dynamics of exposed individuals ($E_H + E_{PEP}$) over short-term periods, where lower τ (indicating stronger memory effects in the fractal-fractional model) leads to more volatile oscillations in exposure levels, reflecting delayed progression (σ_1, σ_2) and prophylaxis failures ($(1-\varepsilon_1)\lambda_H$, $(1-\varepsilon_2)\sigma_2$). This implies that incorporating noninteger derivatives captures realistic heterogeneities in HIV exposure, suggesting interventions like enhanced PEP (θ) could dampen surges in high-memory scenarios to prevent rapid accumulation of latently infected populations. Figure 10b presents a three-dimensional surface plot with time (days) from 0 to 40 on one axis, fractional order τ from 0.55 to 0.95 on another, and total exposed ($E_H + I_H + E_{PEP}$) – likely a summation including treated or related classes – ranging from 5.84×10^6 to 6.00×10^6. Colored from dark blue/purple (low) to yellow (high), the surface rises with time in a jagged, oscillatory manner, with denser ridges at lower τ and a more gradual incline at higher values, exhibiting persistent fluctuations along both time and τ. Figure 10b illustrates how fractional order τ influences the combined exposed and infected compartments ($E_H + I_H + E_{PEP}$), with lower τ amplifying cyclic behaviors due to the Mittag-Leffler kernel's memory in transitions ($\sigma_1 \to I_H$, $\theta_1 \to T_H$), highlighting that fractal-fractional modeling reveals sustained epidemic waves in HIV progression. This signifies the biological advantage of higher τ (closer to integer-order) for stabilizing infection loads, underscoring the need for timely ART (θ_1, θ_2) to mitigate memory-driven rebounds in viral spread. Figure 11a depicts a three-dimensional surface plot with axes for Time (days) 0 to 40, Fractional Order τ 0.55 to 0.95, and Total Susceptible ($S_H + S_{PrEP}$) from -1.50×10^6 to 1.00×10^6, though negative values may indicate modeling artifacts or scaling issues. The color transitions from purple (negative/low) to yellow (high), forming a declining surface with oscillatory ridges that deepen over time, more pronounced at lower τ, resembling a descending, wavy plane with irregular drops. Figure 11a explores the evolution of susceptible populations ($S_H + S_{PrEP}$) under fractional dynamics, where lower τ exacerbates depletions due to intensified force of infection λ_H and PrEP transitions (ω_H), potentially leading to unrealistic negatives as artifacts of numerical simulation. This biologically emphasizes that fractal memory effects accelerate susceptibility loss through exposure, advocating for boosted PrEP efficacy (ε_1) and entry rates (Λ) to sustain population resilience against cyclic HIV incursions. Figure 12a shows a three-dimensional surface plot with γ_H (Contact rate) from 0 to 1.0, γ (Number of partners) from 0 to 10, and R_0 modification factor from 0 to 8.

The surface uses a color gradient from purple (low) to red (high), rising steeply in a block-like manner with higher values at elevated γ_H and γ, forming a smooth, ascending plateau with minimal oscillations. Figure 12a highlights the synergistic effect of contact rate γ_H and partner number γ on the basic reproduction number R_{0H} modification, where increases in both amplify transmission potential via $\lambda_H = \frac{(1-\varsigma\Psi)\gamma\gamma_H(I_H+A+\eta T_H)}{N}$, leading to epidemic thresholds. This implies that behavioral interventions reducing γ or γ_H (e.g., education on safer practices) are crucial to cap R_{0H} below unity, preventing sustained HIV outbreaks in high-risk networks.
Figure 12b is a three-dimensional surface plot with σ_1 (Progression rate of exposed individuals) from 2.0 to 6.0, ρ_1 (Progression rate to AIDS) from 0.00 to 0.14, and R_0 from 0 to 3.0. Colored from blue (low) to yellow (high), the surface appears as a stepped, blocky incline with dotted or grid-like patterns, peaking at higher σ_1 and lower ρ_1, with a relatively flat high region transitioning to lows. Biologically, Figure 12b examines how progression rates σ_1 (from E_H) and ρ_1 (from I_H to A) modulate R_{0H}, with faster σ_1 elevating reproduction by shortening latency and increasing infectious periods, while higher ρ_1 tempers it via quicker AIDS advancement and mortality (δ_A). This biologically suggests optimizing diagnostic timing to slow σ_1 and ρ_1, thereby reducing overall transmissibility and averting progression to severe stages in HIV dynamics. Figure 13a displays a three-dimensional surface plot with ε_1 (Efficacy of PrEP) from 0 to 1.0, ε_2 (Efficacy of PEP)/η (modification for treatment) from 0 to 0.8, and R_0 modification factor from 0 to 7. The color shifts from dark blue (low) to yellow (high), forming a layered, block-like structure with higher values at lower efficacies, exhibiting stepwise increases along the axes. Figure 13a reveals the interplay of PrEP efficacy ε_1, PEP efficacy ε_2, and treatment reduction η, where lower efficacies inflate R_{0H} by heightening failure rates ($(1-\varepsilon_1)\lambda_H$, $(1-\varepsilon_2)\sigma_2$) and sustaining infectivity in T_H. This indicates that enhancing prophylactic and therapeutic efficacies synergistically suppresses reproduction, biologically supporting integrated strategies to minimize exposure transitions and achieve epidemic control. Figure 13b illustrates a three-dimensional surface plot (representing four dimensions via color) with ς (Compliance rate for condom usage) from 0 to 1.0, Ψ (Efficacy of condoms) from 0 to 0.8, and θ_H (Natural mortality) from 0.0100 to 0.0275, with R_0 from 0 to 5 colored blue (low) to yellow (high). The surface forms a grid of blocky elevations, peaking at low ς/Ψ and high θ_H, with segmented layers. Figure 13b assesses how condom adherence ς, efficacy Ψ, and mortality θ_H affect R_{0H}, with poor condom metrics boosting transmission through $(1-\varsigma\Psi)$ in λ_H, while higher θ_H counterintuitively lowers R_{0H} by removing individuals faster. This biologically underscores promoting condom use to reduce effective contacts, outweighing mortality effects, for long-term HIV containment in populations. Figure 14b is a two-dimensional line plot with Basic Reproduction Number R_{0H} from 1.0 to 4.0 on the y-axis and Time (months) from 0 to 25 on the x-axis. Curves are color-coded for γ_H (Contact rate): $\gamma_H = 0.3$ (blue), 0.4 (orange), 0.5 (green), 0.6 (red), 0.7 (purple), showing sinusoidal

oscillations with a period of about 10 months, where higher γ_H yields greater amplitudes and peaks up to 3.8. Figure 14b shows the sensitivity of R_{0H} to contact rate γ_H, with increases intensifying oscillatory transmission due to elevated λ_H, signifying periodic epidemic resurgences. This highlights the biological imperative for contact-reducing measures (e.g., social distancing or education) to flatten curves and maintain R_{0H} below critical thresholds. Figure 15a presents a two-dimensional line plot with R_{0H} from 2.0 to 4.0 on the y-axis and Time (months) 0 to 25 on the x-axis. Parameter Ψ (Condom efficacy) varies: $\Psi = 0.3$ (blue), 0.5 (orange), 0.7 (green), 0.8 (red), 0.9 (purple), with oscillations of 10-month periods, lower Ψ corresponding to higher peaks and amplitudes. Figure 15a indicates that diminishing condom efficacy Ψ escalates R_{0H} fluctuations via weakened protection in $(1 - \varsigma\Psi)$, promoting cyclic infections. This biologically advocates for high-efficacy prophylactics to stabilize dynamics and curb HIV spread over time. Figure 15b depicts a two-dimensional line plot with R_{0H} from 0.5 to 4.5 on the y-axis and Time (months) 0 to 25 on the x-axis. Curves for ε_1 (PrEP effectiveness): $\varepsilon_1 = 0.5$ (blue), 0.6 (orange), 0.7 (green), 0.8 (red), 0.9 (purple), exhibiting sinusoidal waves with 10-month cycles, higher ε_1 linked to lower overall levels and damped amplitudes. Biologically, Figure 15b demonstrates that boosting PrEP effectiveness ε_1 mitigates R_{0H} oscillations by reducing failure to exposure $((1-\varepsilon_1)\lambda_H)$, leading to smoother epidemic control. This signifies the biological value of advanced PrEP formulations in preventing periodic HIV upticks and achieving sustained suppression.

The Figure 16a depicts a two-dimensional line plot with the basic reproduction number R_{0H} on the y-axis ranging from approximately 1.0 to 3.5 and time in months on the x-axis spanning 0 to 25. Multiple colored curves represent different values of the parameter γ (number of sexual partners per individual), specifically $\gamma = 2.0$ (blue), $\gamma = 3.0$ (orange), $\gamma = 4.0$ (green), $\gamma = 5.0$ (red), and $\gamma = 6.0$ (purple). Each curve exhibits sinusoidal oscillations with a consistent period of about 10 months, starting at higher initial values for larger γ (around 3.2 for $\gamma = 6.0$) and decreasing in amplitude over time, though the oscillations persist without fully damping to equilibrium. Biologically, the Figure 16a illustrates the sensitivity of the basic reproduction number R_{0H} to variations in γ, highlighting how an increase in the average number of sexual partners amplifies the oscillatory behavior and elevates the overall transmission potential of HIV/AIDS. Higher γ values lead to greater force of infection $\lambda_H = \frac{(1-\varsigma\Psi)\gamma\gamma_H(I_H+A+\eta T_H)}{N}$, resulting in more pronounced peaks in R_{0H}, which signify periods of heightened epidemic risk; this underscores the importance of interventions reducing partner concurrency to mitigate cyclic surges in infection rates. Figure 16b shows a two-dimensional line plot with R_{0H} on the y-axis from about 1.5 to 3.5 and time in months on the x-axis from 0 to 25. Curves are color-coded for different values of χ (rate of reversion to the HIV-only group due to reduced viral load), including $\chi = 0.05$ (blue), $\chi = 0.1$ (orange), $\chi = 0.15$ (green), $\chi = 0.2$ (red), and $\chi = 0.25$ (purple). The lines display oscillatory patterns with a period of roughly 10 months, where higher χ corresponds to higher

amplitude and peak values, starting near 3.3 for $\chi = 0.25$ and showing slight damping over time. Figure 16b demonstrates that increasing the reversion rate χ from treatment T_H back to I_H exacerbates fluctuations in R_{0H}, as it allows more individuals to re-enter the infectious pool without sustained viral suppression, thereby prolonging epidemic waves; this emphasizes the need for improved treatment adherence to minimize such reversions and stabilize transmission dynamics. Figure 17a presents a two-dimensional line plot with R_{0H} scaled from 1.8 to 3.0 on the y-axis and time from 0 to 25 months on the x-axis. Parameter Θ (reduced disease-induced mortality in the treatment group) varies across curves: $\Theta = 0.3$ (blue), $\Theta = 0.4$ (orange), $\Theta = 0.5$ (green), $\Theta = 0.6$ (red), and $\Theta = 0.7$ (purple). Oscillations are evident with a period of about 10 months, and higher Θ values yield lower overall R_{0H} levels and reduced oscillation amplitudes, indicating a stabilizing effect. Biologically, Figure 17a reveals that enhancing Θ, which lowers mortality in treated individuals via $\Theta\delta_T$, dampens R_{0H} oscillations and reduces average transmission rates by prolonging survival in T_H with lower infectivity ($\eta < 1$), suggesting that therapies improving survival outcomes can help control epidemic cycles and lower long-term prevalence. Figure 17b is a two-dimensional line plot featuring R_{0H} from 1.8 to 3.0 on the y-axis and time from 0 to 25 months on the x-axis. It varies δ_I (disease-induced mortality rate for HIV-infected individuals): $\delta_I = 0.03$ (blue), $\delta_I = 0.04$ (orange), $\delta_I = 0.05$ (green), $\delta_I = 0.06$ (red), and $\delta_I = 0.07$ (purple). The curves oscillate sinusoidally with a 10-month period, where higher δ_I correlates with lower peak R_{0H} and milder fluctuations. Figure 17b indicates that elevating δ_I in the I_H compartment reduces R_{0H} by removing infectious individuals faster, thereby shortening infectious periods and attenuating epidemic oscillations; this highlights the dual-edged role of disease mortality in curbing spread, though ethically, interventions should focus on prevention rather than relying on higher death rates. Figure 18a displays a two-dimensional line plot with R_{0H} ranging from 1.8 to 2.8 on the y-axis and time from 0 to 25 months on the x-axis. Parameter δ_A (disease-induced mortality for HIV/AIDS individuals) is varied: $\delta_A = 0.15$ (blue), $\delta_A = 0.175$ (orange), $\delta_A = 0.2$ (green), $\delta_A = 0.225$ (red), and $\delta_A = 0.25$ (purple). Oscillatory behavior persists with a period of approximately 10 months, and increasing δ_A slightly lowers the average R_{0H} and oscillation intensity.

Biologically, Figure 18a shows that higher δ_A in the A compartment marginally suppresses R_{0H} fluctuations by accelerating removal of advanced-stage infectives, reducing their contribution to λ_H; however, the effect is less pronounced than for earlier stages, implying that targeting progression rates like ρ_1 may be more effective for biological control. Figure 18b illustrates a two-dimensional line plot with R_{0H} from 1.8 to 3.0 on the y-axis and time from 0 to 25 months on the x-axis. It parameterizes δ_T (disease-induced mortality for treated individuals): $\delta_T = 0.01$ (blue), $\delta_T = 0.015$ (orange), $\delta_T = 0.02$ (green), $\delta_T = 0.025$ (red), and $\delta_T = 0.03$ (purple). The

lines exhibit 10-month periodic oscillations, with higher δ_T leading to elevated R_{0H} peaks due to shorter treatment durations. Figure 18b suggests that increasing δ_T amplifies R_{0H} oscillations by diminishing the benefits of treatment in T_H, as faster mortality limits the low-infectivity period (ηT_H); this biologically stresses the value of therapies that minimize δ_T to extend suppressive effects and stabilize epidemic trajectories. Figure 19a is a three-dimensional surface plot with axes labeled as Exposed Class (E_H) Population (0 to 1000), HIV-Only Class (I_H) Population (0 to 1000), and Treated Class (T_H/A) Population (0 to 1000), using a color gradient from purple (low, ∼50) to yellow (high, ∼350) representing AIDS Class Population. The surface forms a sloped, uneven block rising sharply along the Treated Class axis and more gradually along others, with higher AIDS populations in regions of low exposure and high treatment/HIV-only. Biologically, Figure 19a explores interactions among exposed (E_H), HIV-only (I_H), and treated/AIDS ($T_H + A$) compartments, showing that AIDS prevalence escalates when treatment coverage is high but exposure and untreated HIV are low, possibly due to prolonged survival leading to accumulation in later stages; this signifies the need for balanced interventions addressing early exposure (σ_1) and treatment transitions (θ_1, θ_2) to prevent AIDS buildup. Figure 19b depicts a three-dimensional surface plot with axes for Susceptible on PrEP (S_{PREP}) Population (0 to 1000), Exposed on PEP (E_{PEP}) Population (0 to 1000), and HIV-Only Class (I_H) Population (0 to 1000), colored from blue (low, ∼50) to yellow (high, ∼350) for AIDS Class Population. The surface appears as a steep, block-like incline, with AIDS population peaking at high S_{PREP} and low E_{PEP}/I_H, forming a nearly flat high plateau transitioning to lower values. Figure 19b (interpreting the color as a fourth dimension) highlights how prophylactic strategies interact with infection stages, where high PrEP coverage (S_{PrEP}) correlates with elevated AIDS if PEP usage (E_{PEP}) and untreated HIV (I_H) are minimal, suggesting potential gaps in progression management post-prophylaxis failure ($(1-\varepsilon_1)\lambda_H, (1-\varepsilon_2)\sigma_2$); this biologically implies optimizing ε_1 and ε_2 to reduce downstream AIDS despite strong prevention.

4.7 Advantages of the fractal-fractional order method over classical integer-order models in HIV/AIDS modeling

The fractal-fractional order method offers significant advantages over classical integer-order differential equation models when analyzing complex, real-world HIV epidemics. First, it incorporates memory effects through the fractional derivative (order $\tau \in (0, 1]$), capturing how past infections, delayed treatment initiation, and behavioral risk history influence current transmission dynamics—critical in HIV where immune memory and cumulative exposure shape progression

and infectivity. Second, the fractal dimension (parameter ψ) models heterogeneous contact patterns in sexual or injection networks, reflecting clustered risk behaviors (e.g., in key populations) that integer-order models assume away via mean-field approximations. Third, this dual structure yields more accurate long-term predictions, particularly in simulating slow-decaying tails of incidence under partial intervention coverage—patterns observed in mature epidemics but missed by exponential decay in classical models. Fourth, the framework better reproduces empirical data from cohort studies showing non-Markovian progression and sub-exponential growth, enhancing model validation and credibility. Finally, from a public health perspective, it provides superior scenario analysis for combination prevention: It reveals how sustained PrEP, ART scale-up, and condom promotion interact over decades to push R_{0H} below unity and avoid backward bifurcation traps—insights essential for achieving and sustaining the UNAIDS 95-95-95 targets by 2030. While computationally intensive, these advantages make the fractal-fractional approach the preferred tool for strategic, evidence-based HIV elimination planning in heterogeneous, memory-dependent populations.

5 Conclusion

The fractal-fractional order model developed in this research offers a robust framework for analyzing HIV/AIDS transmission dynamics, significantly enhancing traditional integer-order models by incorporating fractal-fractional derivatives. These derivatives combine fractional calculus, which captures memory effects and long-term dependencies in disease progression, with fractal geometry, which models self-similar, heterogeneous transmission patterns across diverse population scales. This approach is particularly effective for HIV/AIDS, as it accounts for the nonlocal nature of infection dynamics and complex contact structures, providing a more accurate representation of real-world epidemic behavior. By integrating PrEP, PEP, and ART, the model demonstrates their partial efficacy in reducing the force of infection and overall disease burden. Analytical proofs confirm solution positivity, boundedness, and global asymptotic stability at the endemic equilibrium when $R_{0H} > 1$. Sensitivity analysis underscores the critical influence of natural mortality, progression rates, contact rates, and treatment initiation on transmission dynamics, while parameter fitting to South African data validates the model's predictive power, forecasting a substantial 28% decline in new infections by 2033 with sustained ART coverage. Numerical simulations further reveal that lower fractional orders intensify oscillatory behaviors in infected compartments, emphasizing the need for consistent prophylactic adherence and early treatment to prevent epidemic resurgence. Compared to integer-order models, the fractal-fractional framework better fits empirical data and offers deeper insights into multi-scale

dynamics, informing optimized resource allocation for epidemic control. Future extensions could incorporate spatial heterogeneity and emerging viral variants to enhance the model's applicability. Numerical simulations reveal that enhancing the synergistic effects of condoms, prophylaxis, and antiretroviral drugs will significantly reduce the burden of HIV/AIDS in the human population.

Recommendations for the Public

1. Sustain and expand ART access to ensure consistent treatment, particularly in high-prevalence regions like South Africa, by reducing cost, stigma, and logistical barriers.

2. Promote consistent PrEP and PEP use through community outreach and subsidized access to reduce infection rates in high-risk groups.

3. Enhance early testing and diagnosis through intensified HIV testing campaigns to prevent progression to AIDS and reduce transmission risk.

4. Reduce high-risk contact behaviors, such as multiple sexual partners, by promoting safe practices like condom use through targeted education.

5. Support long-term adherence to interventions to prevent epidemic resurgence, emphasizing consistent treatment and prophylaxis commitment.

5.1 Limitations of the Model

The fractal-fractional order approach, while powerful in capturing memory effects, behavioral heterogeneity, and long-term dynamics in HIV transmission, has several important limitations. First, the method introduces additional parameters (fractional order τ and fractal dimension ψ), which require careful calibration using longitudinal cohort or surveillance data—data that are often incomplete or unavailable in low-resource settings. Misestimation of these parameters can lead to biased projections of R_{0H}, equilibrium prevalence, or intervention impact. Second, the increased computational complexity of solving fractal-fractional systems—especially with the Adams–Bashforth scheme—demands significant processing power and time, limiting real-time forecasting during public health emergencies. Third, interpretability is reduced; while the model better reflects biological and social realism, the noninteger derivatives obscure direct causal links, making it harder for policymakers to translate results into intuitive action. Finally,

the assumption of uniform memory and fractal structure across populations may oversimplify local variations in risk behavior, treatment adherence, or viral evolution. These limitations suggest that while the fractal-fractional framework is valuable for strategic long-term planning and theoretical insight, it should be complemented with simpler integer-order models for rapid response and sensitivity analyses for parameter uncertainty in operational decision-making.

Areas for Future Research

1. Incorporate spatial heterogeneity into the HIV/AIDS model.
2. Model emerging HIV/AIDS variants.
3. Integrate stochastic effects into the model
4. Explore neural network enhancements.
5. Analyze time-dependent optimal control measures on the HIV/AIDS model.

Funding

This research received no external funding.

Conflicts of Interest

The author declares no conflicts of interest.

References

[1] Acheneje, G. O., Omale, D., Atokolo, W. and Bolaji, B., *Modeling the transmission dynamics of the co-infection of COVID-19 and monkeypox diseases with optimal control strategies and cost–benefit analysis*, Franklin Open, 8 (2024), 100130.

[2] Acheneje, G. O., Omale, D., Atokolo, W., Celestine, A. B., Abah, E., Dervishi, R., Shyamsunder and Bolaji, B., *Mathematical modelling on the transmission dynamics of the co-infection of COVID-19 and monkeypox with treatment as a control strategy*, Discov. Public Health, 22(1) (2025), 535.

[3] Agarwal, P., Jleli, M. and Samet, B., *Fixed point theory in metric spaces: recent advances and applications*, Springer, Singapore, 2018.

[4] Ahmad, S., Ullah, A., Shah, K., Salahshour, S., Ahmadian, A. and Ciano, T., *Fuzzy fractional-order model of the novel coronavirus*, Adv. Differ. Equ., 1 (2020), 1–17.

[5] Anderson, P. L., Glidden, D. V., Liu, A., Buchbinder, S., Lama, J. R., Guanira, J. V. and Grant, R. M., *Emtricitabine–tenofovir concentrations and pre-exposure prophylaxis efficacy in men who have sex with men*, Sci. Transl. Med., 4(151) (2012), 151ra125.

[6] Anderson, R. M. and May, R. M., *Infectious diseases of humans: dynamics and control*, Oxford University Press, Oxford, 1991.

[7] Arafa, A. A. M., Rida, S. Z. and Khalil, M., *Fractional modeling dynamics of HIV and $CD4^+$ T-cells during primary infection*, Nonlinear Biomed. Phys., 6(1) (2012), 1–7.

[8] Atangana, A., *Fractal–fractional differentiation and integration: connecting fractal calculus and fractional calculus to predict complex systems*, Chaos Solitons Fractals, 102 (2017), 396–406.

[9] Atangana, A., *Fractional operators with constant and variable order with application to geo-hydrology*, Academic Press, London, 2017.

[10] Atangana, A. and Baleanu, D., *New fractional derivatives with nonlocal and non-singular kernel: theory and application to heat transfer model*, Therm. Sci., 20(2) (2016), 763–769.

[11] Atangana, A. and Qureshi, S., *Modeling attractors of chaotic dynamical systems with fractal–fractional operators*, Chaos Solitons Fractals, 123 (2019), 320–337.

[12] Atokolo, W., Aja, R. O., Omale, D., Ahman, Q. O., Acheneje, G. O. and Amos, J., *Fractional mathematical model for the transmission dynamics and control of Lassa fever*, Franklin Open, 7 (2024), 100110.

[13] Baleanu, D., Jajarmi, A., Mohammadi, H. and Rezapour, S., *A new study on the mathematical modelling of human liver with Caputo–Fabrizio fractional derivative*, Chaos Solitons Fractals, 134 (2020), 109705.

[14] Bekker, L. G., Johnson, L., Cowan, F., Overs, C., Besada, D., Hillier, S. and Cates Jr., W., *Combination HIV prevention for female sex workers: what is the evidence?*, Lancet, 385(9962) (2015), 72–87.

[15] Bhunu, C. P. and Mushayabasa, S., *Modelling the transmission dynamics of HIV/AIDS and hepatitis B co-infection*, HIV AIDS Rev., 11(4) (2012), 118–124.

[16] Blower, S. M. and Dowlatabadi, H., *Sensitivity and uncertainty analysis of complex models of disease transmission: an HIV model as an example*, Int. Stat. Rev., 62(2) (1994), 229–243.

[17] Bolaji, B., Ibrahim, A., Ani, F., Omede, B. and Acheneje, G., *A model for the control of transmission dynamics of human monkeypox disease in Sub-Saharan Africa*, J. Niger. Soc. Phys. Sci., 6 (2024), 1800.

[18] Bryant, J., Baxter, L. and Hird, S., *Non-occupational post-exposure prophylaxis for HIV: a systematic review*, Health Technol. Assess., 17(20) (2013), 1–195.

[19] Cardo, D. M., Culver, D. H., Ciesielski, C. A., Srivastava, P. U., Marcus, R., Abiteboul, D. and McKibben, P. S., *A case–control study of HIV seroconversion in health care workers after percutaneous exposure*, N. Engl. J. Med., 337(21) (1997), 1485–1490.

[20] Cohen, M. S., Chen, Y. Q., McCauley, M., Gamble, T., Hosseinipour, M. C., Kumarasamy, N. and Fleming, T. R., *Prevention of HIV-1 infection with early antiretroviral therapy*, N. Engl. J. Med., 365(6) (2011), 493–505.

[21] Cohen, M. S., Chen, Y. Q., McCauley, M., Gamble, T., Hosseinipour, M. C., Kumarasamy, N. and Godbole, S. V., *Antiretroviral therapy for the prevention of HIV-1 transmission*, N. Engl. J. Med., 375(9) (2016), 830–839.

[22] Davarian, N., Heydari, A., Hashemi Mehne, S. H. and Heydari, A. A., *The investigation of stability and optimal control of the multigroup COVID-19 epidemic model in Iran*, J. Math. Ext., 19(1) (2025), 1–20.

[23] Deeks, S. G., Overbaugh, J., Phillips, A. and Buchbinder, S., *HIV infection*, Nat. Rev. Dis. Primers, 1(1) (2015), 1–22.

[24] Ding, Y., Wang, Z. and Ye, H., *Optimal control of a fractional-order HIV-immune system with memory*, IEEE Trans. Control Syst. Technol., 20(3) (2012), 763–769.

[25] French, P. P., Latka, M., Gollub, E. L., Rogers, C., Hoover, D. R. and Stein, Z. A., *Use-effectiveness of the female versus male condom in preventing sexually transmitted disease in women*, Sex. Transm. Dis., 30(5) (2003), 433–439.

[26] Grant, R. M. and Glidden, D. V., *HIV moments and pre-exposure prophylaxis*, Lancet, 387(10027) (2016), 1507–1508.

[27] Grant, R. M., Lama, J. R., Anderson, P. L., McMahan, V., Liu, A. Y., Vargas, L. and Glidden, D. V., *Preexposure chemoprophylaxis for HIV prevention in men who have sex with men*, N. Engl. J. Med., 363(27) (2010), 2587–2599.

[28] Khan, M. A., Ullah, S. and Farhan, M., *The dynamics of Zika virus with Caputo fractional derivative*, AIMS Math., 4(1) (2020), 134–154.

[29] Kilbas, A. A., Srivastava, H. M. and Trujillo, J. J., *Theory and applications of fractional differential equations*, Elsevier, Amsterdam, 2006.

[30] Kuhar, D. T., Henderson, D. K., Struble, K. A., Heneine, W., Thomas, V., Cheever, L. W. and Panlilio, A. L., *Updated US public health service guidelines for the management of occupational exposures to HIV and recommendations for postexposure prophylaxis*, Infect. Control Hosp. Epidemiol., 34(9) (2013), 875–892.

[31] Kumar, S., Kumar, R., Cattani, C. and Samet, B., *Chaotic behaviour of fractional predator–prey dynamical system*, Chaos Solitons Fractals, 135 (2020), 109811.

[32] La Salle, J. P., *The stability of dynamical systems*, SIAM, Philadelphia, 1976.

[33] Odiba, P., Acheneje, G. O. and Bolaji, B., *A compartmental deterministic epidemiological model with nonlinear differential equations for analyzing the co-infection dynamics between COVID-19, HIV and monkeypox diseases*, Healthc. Anal., 5 (2024), 100311.

[34] Omame, A., Han, Q., Iyaniwura, S. A., Ebenezer, A., Bragazzi, N. L., Wang, X. and Woldegerima, W. A., *Understanding the impact of HIV on mpox transmission in the MSM population: a mathematical modeling study*, Infect. Dis. Model., 9(4) (2024), 1117–1137.

[35] Owolabi, K. M. and Atangana, A., *Mathematical analysis and computational experiments for an epidemic system with nonlocal and nonsingular derivative*, Chaos Solitons Fractals, 126 (2019), 41–49.

[36] Owolabi, K. M. and Atangana, A., *Fractal fractional-order derivative for HIV/AIDS model with Mittag–Leffler kernel*, Alexandria Eng. J., 61 (2022), 10965–10980.

[37] Palella Jr., F. J., Delaney, K. M., Moorman, A. C., Loveless, M. O., Fuhrer, J., Satten, G. A. and Holmberg, S. D., *Declining morbidity and mortality among patients with advanced human immunodeficiency virus infection*, N. Engl. J. Med., 338(13) (1998), 853–860.

[38] Perelson, A. S., *Modelling viral and immune system dynamics*, Nat. Rev. Immunol., 2(1) (2002), 28–36.

[39] Potts, M., Halperin, D. T., Kirby, D., Swidler, A., Marseille, E., Klausner, J. D. and Gayle, H., *Reassessing HIV prevention*, Science, 320(5877) (2008), 749–750.

[40] Rodger, A. J., Cambiano, V., Bruun, T., Vernazza, P., Collins, S., Degen, O. and Lundgren, J., *Sexual activity without condoms and risk of HIV transmission in serodifferent couples when the HIV-positive partner is using suppressive antiretroviral therapy*, JAMA, 316(2) (2016), 171–181.

[41] Shah, K., Alqudah, M. A., Jarad, F. and Abdeljawad, T., *Semi-analytical study of Pine Wilt Disease model with convex rate under Caputo–Fabrizio fractional order derivative*, Chaos Solitons Fractals, 135 (2020), 109754.

[42] Smart, D. R., *Fixed point theorems*, Cambridge University Press, Cambridge, 1974.

[43] Sharp, P. M. and Hahn, B. H., *Origins of HIV and the AIDS pandemic*, Cold Spring Harb. Perspect. Med., 1(1) (2011), a006841.

[44] Toufik, M. and Atangana, A., *New numerical approximation of fractional derivative with non-local and non-singular kernel: application to chaotic models*, Eur. Phys. J. Plus, 132(10) (2017), 444.

[45] UNAIDS, *Global HIV & AIDS statistics: fact sheet*, Joint United Nations Programme on HIV/AIDS, 2021.

[46] UNAIDS, *2024 UNAIDS global AIDS update summary for South Africa*, Joint United Nations Programme on HIV/AIDS, 2024.

[47] Van Den Driessche, P. and Watmough, J., *Reproduction numbers and sub-threshold endemic equilibria for compartmental models of disease transmission*, Math. Biosci., 180(1–2) (2002), 29–48.

[48] Weller, S. and Davis, K., *Condom effectiveness in reducing heterosexual HIV transmission*, Cochrane Database Syst. Rev., 1 (2002), CD003255.

[49] World Health Organization, *Guideline on when to start antiretroviral therapy and on pre-exposure prophylaxis for HIV*, World Health Organization, Geneva, 2015.